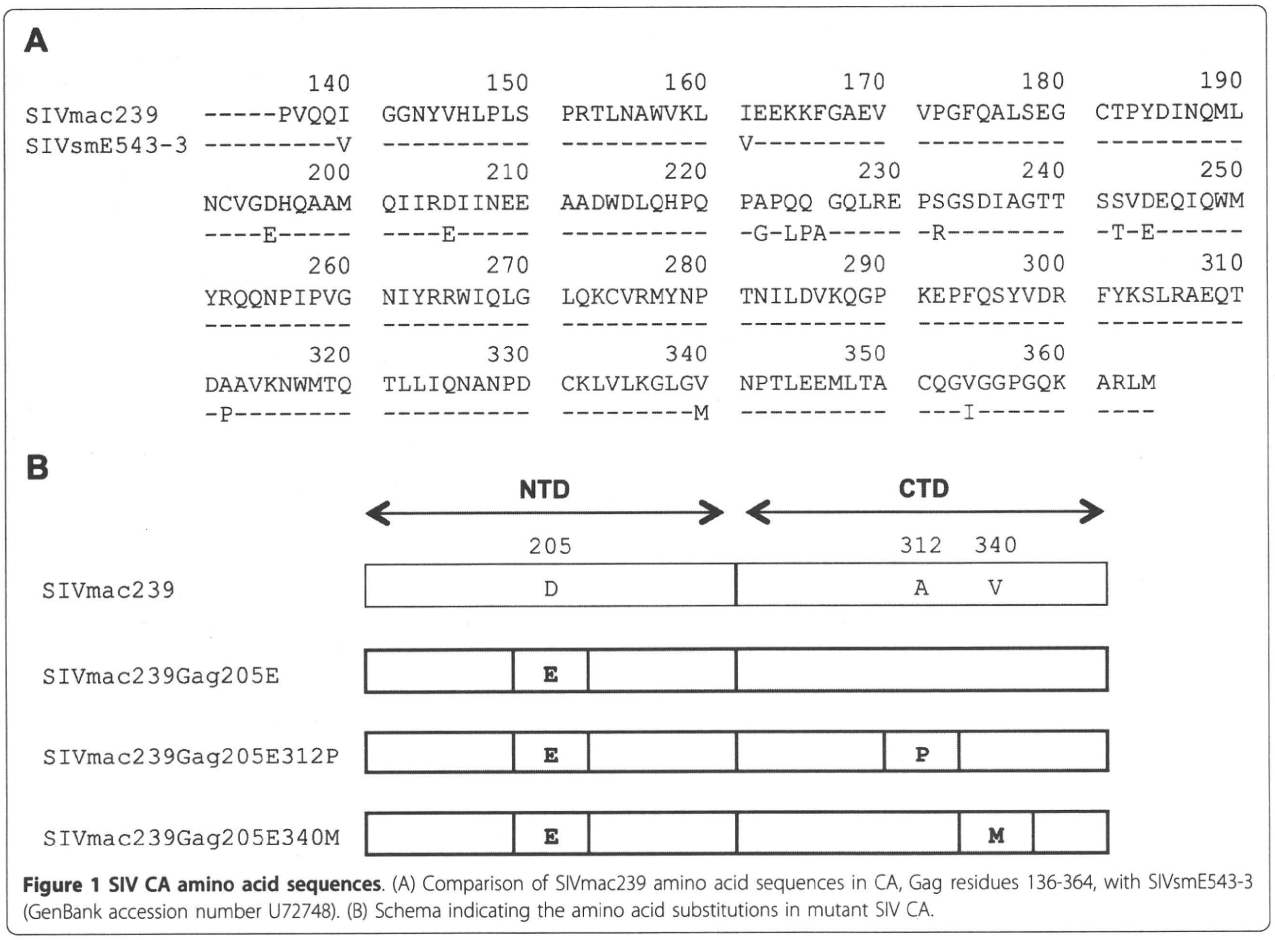

Figure 1 SIV CA amino acid sequences. (A) Comparison of SIVmac239 amino acid sequences in CA, Gag residues 136-364, with SIVsmE543-3 (GenBank accession number U72748). (B) Schema indicating the amino acid substitutions in mutant SIV CA.

Full recovery of viral fitness in SIVmac239Gag205E340M

We then focused on analyzing the possibility of functional interaction between Gag residues 205 in CA NTD and 312/340 in CA CTD. To confirm differences in viral fitness among SIVmac239, SIVmac239Gag205E, SIVmac239Gag205E312P, and SIVmac239Gag205E340M, we compared their replicative ability by viral competition assay (Table 1). The competitions confirmed lower viral fitness of SIVmac239Gag205E compared to wild-type SIVmac239, SIVmac239Gag205E312P, and SIVmac239Gag340M. SIVmac239Gag205E312P showed lower viral fitness than SIVmac239, whereas replication ability of SIVmac239Gag205E340M was no less than the wild-type. These results indicate that the GagD205E substitution in SIVmac239 reduced viral fitness, which was recovered partially by an additional GagA312P and fully by an additional GagV340M substitution. The competition between SIVmac239 and SIVmac239Gag205E340M at the ratio of 1:1 resulted in selection of the latter, suggesting that SIV CA with Gag205E-340M combination observed in SIVsmE543-3 may be slightly more functional than that with Gag205D-340V in SIVmac239.

Inhibition of the early phase of SIVmac239Gag205E replication

We examined whether the GagD205E substitution affects the early or late phase of SIVmac239 replication. On LuSIV cells, SIVmac239Gag205E infection showed significantly lower luciferase activity compared to wild-type SIVmac239, SIVmac239Gag205E312P, or SIVmac239Gag205E340M, indicating suppression of the early phase of SIVmac239GagD205E replication (Figure 5). In contrast, we did not find a significant difference in viral production among SIVmac239, SIVmac239Gag205E, SIVmac239Gag205E312P, and SIVmac239Gag205E340M (Figure 6). These results indicate that the loss of viral fitness by the GagD205E substitution is mainly due to inhibition of the early phase of viral replication.

Loss of in vitro core stability in SIVmac239Gag205E

If the GagD205E substitution disturbs intermolecular CA interaction for hexamer formation, it may affect SIV core stability. To assess the core stability in vitro [34], concentrated viruses were separated into three fractions by ultracentrifugation under gradient sucrose

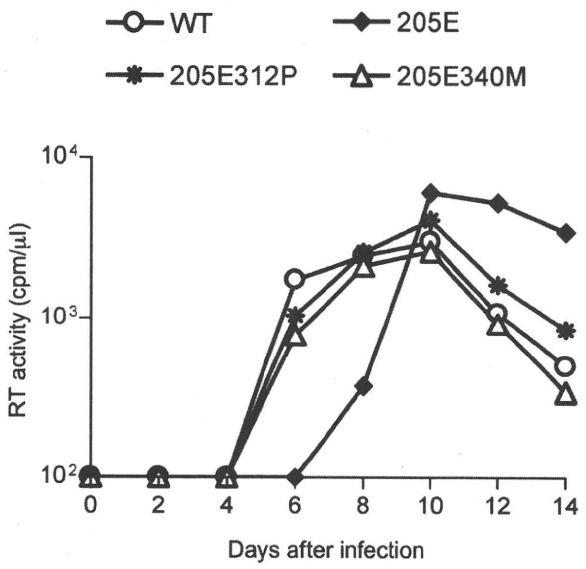

Figure 2 Wild-type and mutant SIV replication kinetics in HSC-F cells. HSC-F cells were infected with SIVmac239 (WT, open circles), SIVmac239Gag205E (205E, closed diamonds), SIVmac239Gag205E312P (205E312P, asterisk), or SIVmac239Gag205E340M (205E340M, open triangles). Virus production was monitored by measuring RT activity in the culture supernatants. A representative result from five sets of experiments is shown.

concentrations in the presence of Triton X-100 and each fraction was subjected to Western blot analysis to detect CA p27 proteins (Figure 7). In the absence of Triton X-100, CA proteins were detected in the bottom fraction, whereas those in the presence of 1% Triton X-100 were sensitive to the detergent and detected not in the bottom but only in the top fraction (data not shown). We compared the in vitro viral core stability between SIVmac239 and SIVmac239Gag205E in the presence of 0.6%, 0.9%, and 1.35% Triton X-100, respectively, and found a difference in the presence of 0.6% Triton X-100. Additional experiments revealed that SIVmac239Gag205E core was more sensitive to 0.6% Triton X-100 treatment than SIVmac239, SIVmac239Gag205E312P, and SIVmac239Gag205E340M (Figure 7). These results suggest that viral core stability may be reduced by GagD205E substitution but can be recovered by additional GagA312P or GagV340M substitution.

Selection of GagD205E plus GagV340M mutations in a SIVmac239-infected macaque

The GagD205E substitution results in viral escape from $Gag_{206\text{-}216}$-specific CTL recognition. Finally, we examined whether this substitution can be selected in the chronic phase of SIVmac239 infection in *90-120-Ia*-positive macaques eliciting $Gag_{206\text{-}216}$-specific CTL responses using plasma samples obtained in our previous experiments [35,36]. SIVmac239-infected *90-120-Ia*-positive macaques select the GagL216S mutation resulting in viral escape from $Gag_{206\text{-}216}$-specific CTL recognition, but we found selection of both GagD205E and GagV340M mutations in viral genomes in one animal, R01-007 (Table 2). In this animal, GagD205E and GagV340M mutations were undetectable at week 123 after SIVmac239 challenge, but both became detectable at week 137 and were dominant at week 150. In contrast, the GagL216S mutation dominant at week 123 was not detected at week 150. These results present in vivo evidence indicating functional interaction between the Gag 205th residue in NTD and the 340th in CTD of SIV CA.

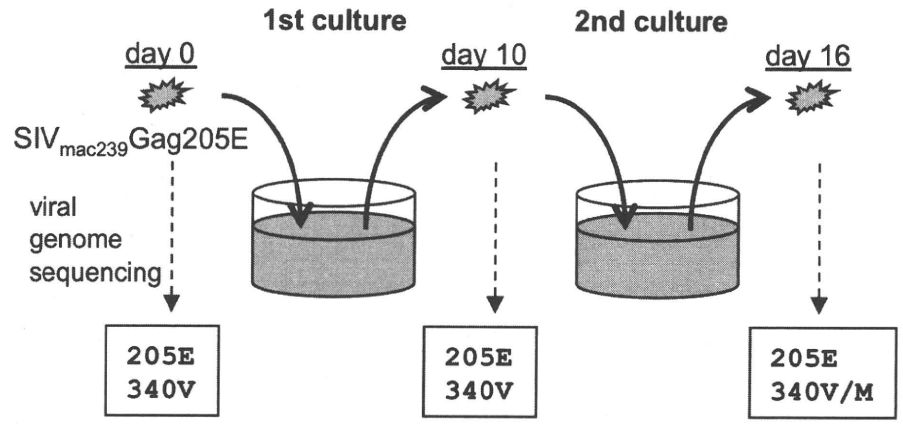

Figure 3 Passage of SIVmac239Gag205E culture supernatants. HSC-F cells were infected with SIVmac239Gag205E. The culture supernatant on day 10 was added to fresh HSC-F cells to start the second culture. Viral RNAs were extracted from the first culture supernatant on day 10 and the second culture supernatant on day 16 after the initial infection and subjected to sequence analyses. Dominant amino acid at the 340th residue remained V on day 10 in all cases but was M on day 16 in two of four sets of experiments (Gag340M was detectable on day 10 in these two sets of experiments). No other amino acid change was observed in the CA-coding region.

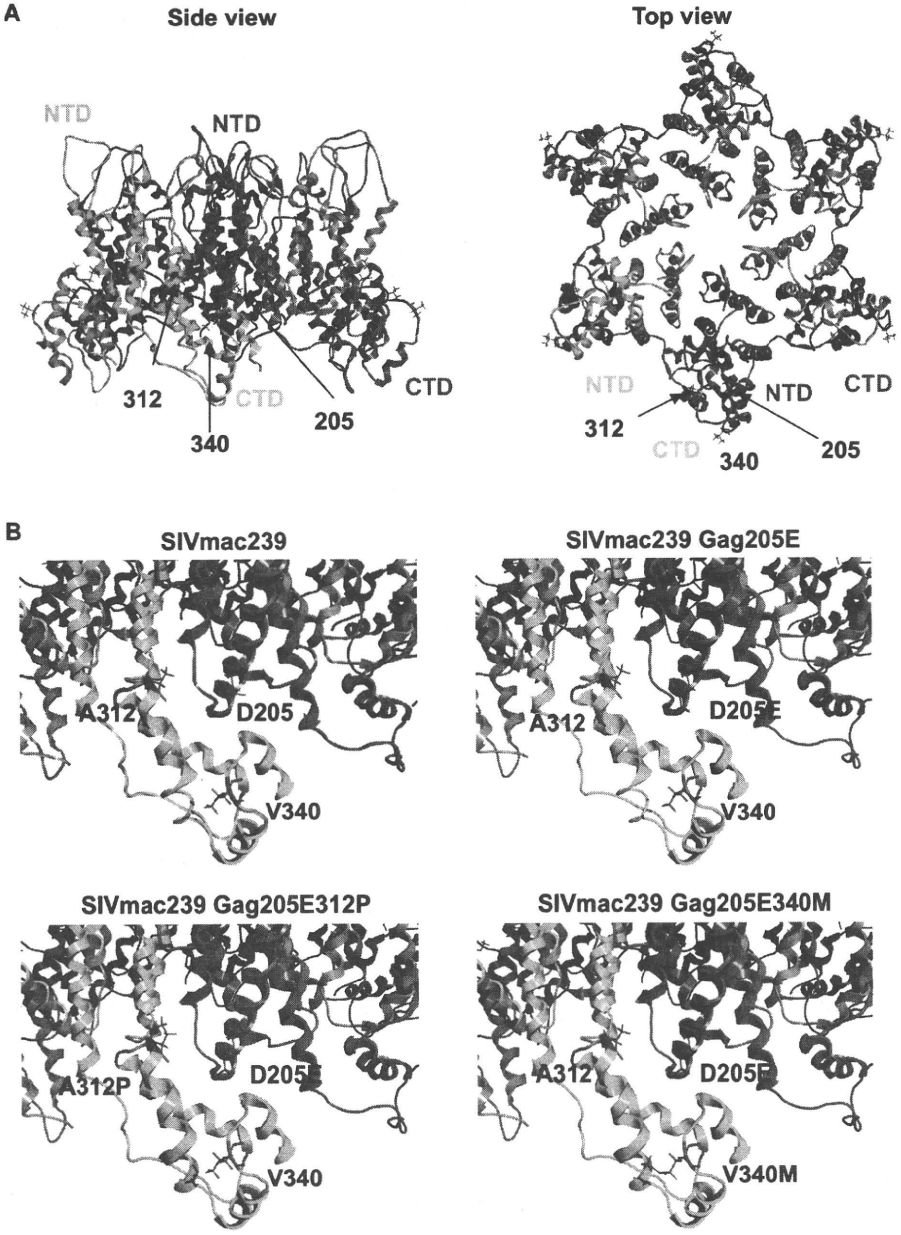

Figure 4 Structural models of SIVmac239 CA hexamer. The hexameric SIVmac239 CA models were constructed by homology-modeling using a crystal structure of the hexameric HIV-1 CA at a resolution of 1.90 Å (PDB code: 3H47[33]) as a modeling template. "MOE-Align" and "MOE-Homology" in MOE version 2008.1002 were used for the modeling. The side chains of the 205th, 312th, and 340th aa in Gag are shown as orange sticks. (A) Overall structure of SIVmac239 CA hexamer. (B) The hexameric structures near positions 205, 312, and 340 of wild-type and mutant SIVmac239 CAs.

Discussion

The Gag CA which is one of the most conserved proteins in HIV and SIV may be a promising immunogen for CTL-based AIDS vaccines. However, the limitations imposed on amino acid sequences in CA are not fully understood. In the present study, we found that the GagD205E substitution in SIVmac239 CA NTD reduces viral fitness, which is recovered by additional GagA312P or GagV340M substitution in the CTD. SIVmac239-Gag205E passaged in cell culture often resulted in selection of an additional GagV340M mutation. Furthermore, selection of Gag205E plus Gag340M mutations, but not Gag205E alone, was observed in a chronically SIVmac239-infected rhesus macaques. These results provide evidence indicating a functional interaction between Gag residues 205 in CA NTD and 340 in CA CTD,

Table 1 Competition between SIV mutants[a]

SIVs in competition	Ratio of inoc. titers[b]	Exp. no.	Dominant aa sequences[c]			
			day 6		day 18	
SIVmac239 & SIVmac239Gag205E	4:1	#1	205D		205D	
		#2	205D		205D	
	1:1	#1	205D		205D	
		#2	205D		205D	
	1:4	#1	205D		205D	
		#2	205D		205D	
SIVmac239 & SIVmac239Gag205E312P	4:1	#1	205D	312A	205D	312A
		#2	205D	312A	205D	312A
	1:1	#1	205D	312A	205D	312A
		#2	205D	312A	205D	312A
	1:4	#1	205D	312A	205D	312A
		#2	205D	312A	205D	312A
SIVmac239 & SIVmac239Gag205E340M	4:1	#1	205D	340V	205D	340V
		#2	205D	340V	205D	340V
	1:1	#1	205D/E	340V/M	205E	340M
		#2	205D/E	340V/M	205E	340M
	1:4	#1	205E	340M	205E	340M
		#2	205E	340M	205E	340M
SIVmac239Gag205E & SIVmac239Gag205E312P	4:1	#1	205E	312P	205E	312P
		#2	205E	312P	205E	312P
	1:1	#1	205E	312P	205E	312P
		#2	205E	312P	205E	312P
	1:4	#1	205E	312P	205E	312P
		#2	205E	312P	205E	312P
SIVmac239Gag205E & SIVmac239Gag205E340M	4:1	#1	205E	340M	205E	340M
		#2	205E	340M	205E	340M
	1:1	#1	205E	340M	205E	340M
		#2	205E	340M	205E	340M
	1:4	#1	205E	340M	205E	340M
		#2	205E	340M	205E	340M

[a]HSC-F cells were coinfected with two kinds of SIVs indicated. Viral *gag* fragments were amplified by RT-PCR from viral RNAs from the culture supernatants on days 6 and 18 postinfection and then sequenced. Results from two sets of experiments (Exp. #1 and #2) are shown.

[b]The ratio of the dose (RT activity) of the virus indicated at the top to that at the bottom at coinfection.

[c]Dominant amino acid sequences at the positions where mutations were included in the inoculums are shown. 205D/E, D and E were detected equally at the 205th aa in Gag; 340 V/M, V and M were detected equally at the 340th aa in Gag.

presenting a structural constraint for functional interaction between SIV CA NTD and CTD.

HIV and SIV Gag proteins are expressed as unprocessed polyproteins, which are assembled and incorporated into the virions. Concomitant with viral budding, incorporated Gag polyproteins are proteolytically cleaved by viral protease into processed proteins including MA (matrix), CA, and NC (nucleocapsid), participating in mature infectious virion formation [37,38]. Recent structural analyses [31-33,39-41] indicated that CA proteins form hexamer lattice in matured virions; in the mature CA core, the intermolecular NTD-NTD and NTD-CTD interfaces are involved in the formation of CA hexamers, while the intermolecular CTD-CTD interface connects neighboring hexamers. Our modeling analyses did not support a possibility of intramolecular interaction but indicated possible intermolecular interaction between Gag205 in CA NTD and Gag312/340 in CA CTD, which may affect CA hexamer formation during viral maturation. This is consistent with our results in Figure 5 indicating that the GagD205E substitution results in inhibition of the early phase of SIVmac239 replication, which can be overcome by additional GagA312P or GagV340M substitution. This possibility is supported also by our results on viral core stability in vitro, although it remains unclear how much extent the

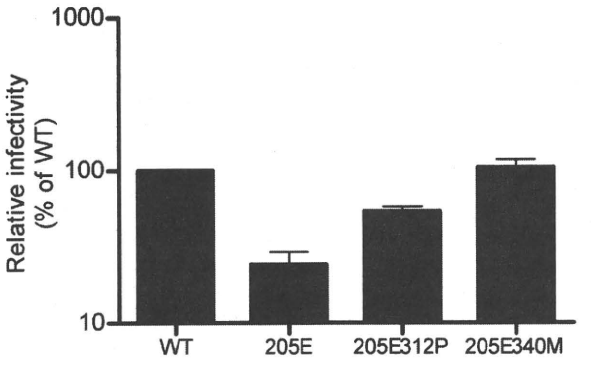

Figure 5 Mutant SIV infection. LuSIV cells were infected with SIVmac239 (WT), SIVmac239Gag205E (205E), SIVmac239Gag205E312P (205E312P), or SIVmac239Gag205E340M (205E340M). Luciferase activity was measured 24 hr after infection. Relative infectivity is shown as the ratio (%) of the luciferase activity to that of SIVmac239 (WT). Mean values in three sets of experiments are shown.

core stability in vitro can reflect the one in vivo [42]. There has been no report suggesting the influence of the Gag 205 residue on SIV sensitivity to tripartite interaction motif 5α (TRIM5α). A previous report on HIV CA lattice [31,43] indicated a potential interaction between the helix 4 of NTD and the loop connecting helices 10 and 11 of CTD in the adjacent molecule. Our results suggest the possible involvement of Gag205 and Gag340 residues in this intermolecular NTD-CTD interaction in CA hexamers.

The molecular model of CA hexamers incorporating the GagD205E substitution suggested shortening of the distance between Gag205 and Gag340 residues, which looked to be compensated by GagV340M substitution (Figure 4). The modeling can draw a hydrophobic pocket between Gag205 and Gag340 residues in

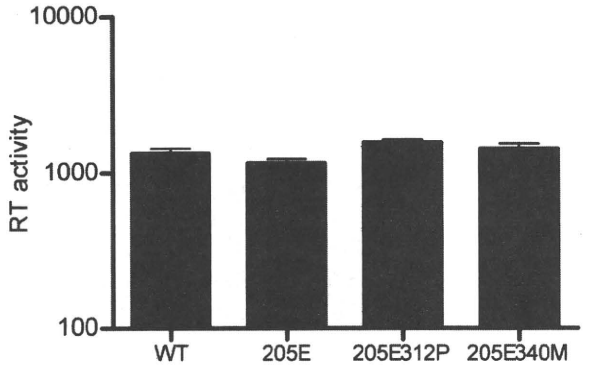

Figure 6 Mutant SIV production. COS-1 cells were transfected with molecular clone DNAs of SIVmac239 (WT), SIVmac239Gag205E (205E), SIVmac239Gag205E312P (205E312P), or SIVmac239Gag205E340 M (205E340 M). RT activity of the culture supernatants two days after transfection was measured. Mean values in five sets of experiments are shown.

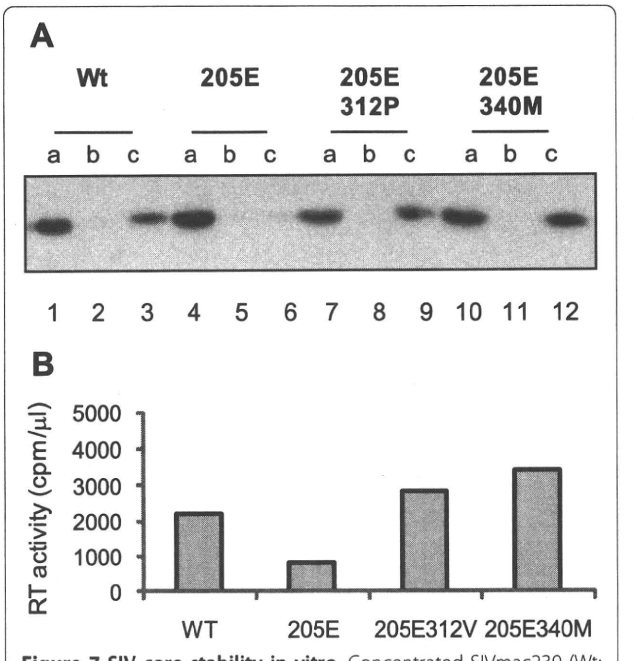

Figure 7 SIV core stability in vitro. Concentrated SIVmac239 (Wt; lanes 1-3), SIVmac239Gag205E (205E; lanes 4-6), SIVmac239Gag205E312P (205E312P; lanes 7-9), or SIVmac239Gag205E340M (205E340 M; lanes 10-12) was separated into three fractions (top [a], middle [b], and bottom [c]) by ultracentrifugation under gradient sucrose concentrations in the presence of 0.6% Triton X-100. Each fraction was subjected to Western blot analysis to detect SIV CA p27 proteins (A). A representative result from three sets of experiments is shown. The bottom (c) fractions were also subjected to RT assay (B).

SIVmac239Gag205E340M as well as SIVmac239, but not in SIVmac239Gag205E CA hexamers. Thus, this pocket may be a target candidate for anti-viral drugs.

Both GagL216S and GagD205E mutations can result in escape from $Gag_{206\text{-}216}$-specific CTL recognition [19,28], but the former is usually selected in SIVmac239-infected *90-120-Ia*-positive macaques probably

Table 2 Viral gag sequences in macaque R01-007 infected with SIVmac239[a]

Wks after challenge	Amino acid sequences[b]		
	at 205th	at 216th	at 340th
123	D	S	V
137	D (E)	S (L)	V (M)
150	E	L	M

[a]Viral RNAs were extracted from plasma obtained from a 90-120-Ia-positive macaque R01-007 at weeks 123, 137, and 150 after SIVmac239 challenge. Viral *gag* fragments were amplified by RT-PCR from viral RNAs and then sequenced. This animal showed efficient $Gag_{206\text{-}216}$-specific CTL responses and vaccine-based control of a SIVmac239 challenge with rapid selection of the GagL216S escape mutation (at week 5), but accumulated viral mutations in the chronic phase, leading to reappearance of plasma viremia around week 60 after challenge as described previously [19,35].

[b]Dominant amino acid sequences at the 205th, 216th, and 340th aa in Gag are shown. Parentheses indicate the sequences that are not dominant but detectable.

because the latter reduces viral fitness more severely than the former. In this study, we found selection of GagD205E plus GagV340M mutations in the chronic phase of SIVmac239 infection in a *90-120-Ia*-positive macaque. In this animal, the CTL escape GagL216S mutation first selected after SIVmac239 challenge became undetectable and was replaced with the CTL escape GagD205E mutation in combination with GagV340M in the chronic phase. This may imply that the GagD205E plus GagV340M mutations might be more advantageous than the GagL216S mutation for SIVmac239 replication in the presence of $Gag_{206-216}$-specific CTL pressure.

We observed the addition of GagV340M mutation but not a Gag205E-to-Gag205D reversion in SIVmac239-Gag205E passage. This may be due to difference in frequencies between purine-to-purine (guanine-to-adenine) change in the former and purine-to-pyrimidine (adenine-to-thymine) change in the latter. The appearance of additional GagV340M mutation in SIVmac239-Gag205E passaged in cell culture as well as the selection of GagD205E plus GagV340M mutations in an animal provides key evidence indicating functional interaction between Gag residues 205 in CA NTD and 340 in CA CTD. The Gag is a promising candidate as a vaccine immunogen for CTL induction, because cumulative studies have indicated the efficacy of Gag-specific CTL responses against HIV and SIV infection [7,25,44,45]. However, viral mutational escape from CTL recognition is a major challenge for AIDS vaccine design. Thus, the information on the structural constraint presented in this study might be helpful for immunogen design in AIDS vaccine development.

Conclusions

Our results present in vitro and in vivo evidence implicating the interaction between Gag residues 205 in CA NTD and 340 in CA CTD in SIV replication. SIV CA with Gag205D-340V (observed in SIVmac239) or Gag205E-340M combination (observed in SIVsmE543-3) is functional whereas the CA with Gag205E-340V is less functional. Thus, the present study indicates a structural constraint for functional interaction between SIV CA NTD and CTD, providing valuable information for immunogen design to limit viral escape options.

Methods

Analysis of mutant SIV replication

SIV molecular clone DNAs with gag mutations were constructed by site-directed mutagenesis from the wild-type SIVmac239 molecular clone DNA [24]. Virus stocks were obtained by transfection of COS-1 cells with wild-type or mutant SIV molecular clone DNAs using Lipofectamine LTX PLUS (Invitrogen, Tokyo, Japan). Viral titers were measured by reverse transcription (RT) assay as described previously [46]. For analysis of viral replication kinetics, HSC-F cells (herpesvirus saimiri-immortalized macaque T-cell line) [47] were infected with wild-type or mutant SIVs (normalized by RT activity), and virus production was monitored by measuring RT activity in the culture supernatants. To examine viral infectivity, LuSIV cells, which are derived from CEMx174 cells and contain a luciferase indicator gene under the control of the SIVmac239 long terminal repeat, were cultured for 24 hr after viral infection and then lysed in a reporter lysis buffer (Promega Corp., Tokyo, Japan) for measurement of the luciferase activity in a luminometer (GloMax™ 96 Microplate Luminometer, Promega Corp.).

Viral competition assay

HSC-F cells were coinfected with two SIVs at a ratio of 1:1 or 1:4, and the culture supernatants harvested every other day were used for RT assays. On day 6, the supernatant was added to fresh HSC-F cells to start the second culture. Similarly, on day 12 after the initial coinfection, the second culture supernatant was added to fresh HSC-F cells to start the third culture. RNAs were extracted using the High Pure viral RNA kit (Roche Diagnostics, Tokyo, Japan) from the initial culture supernatant on day 6 and from the third culture supernatant on day 18 post-coinfection. The fragment (nucleotides 1231 to 2958 in SIVmac239 [GenBank accession number M33262]) containing the entire gag region was amplified from the RNA by RT-PCR and sequenced to determine dominant sequences as described previously [19].

Molecular modeling of hexameric SIVmac239 CA

The crystal structures of HIV-1 CA NTD at a resolution of 2.00 Å (PDB code: 1M9C[48]), HIV-1 CA CTD at a resolution of 1.70 Å (PDB code: 1A8O[5]), and hexameric HIV-1 CA at a resolution of 1.90 Å (PDB code: 3H47 [33]) were taken from the RCSB Protein Data Bank [49]. Three-dimensional (3-D) models of monomeric SIVmac239 CA were constructed by the homology modeling technique using 'MOE-Align' and 'MOE-Homology' in the Molecular Operating Environment (MOE) version 2008.1002 (Chemical Computing Group Inc., Quebec, Canada) as described [50,51]. We obtained 25 intermediate models per one homology modeling in MOE, and selected the 3-D models which were the intermediate models with best scores according to the generalized Born/volume integral methodology [52]. The final 3-D models were thermodynamically optimized by energy minimization using an AMBER99 force field [53] combined with the generalized Born model of aqueous solvation implemented in MOE [54]. Physically unacceptable

local structures of the optimized 3-D models were further refined on the basis of evaluation by the Ramachandran plot using MOE. The structures of hexameric SIVmac239 CA were generated from the monomeric structures by MOE on the basis of the assembly information of hexameric HIV-1 CA crystal structure [33].

Analysis of viral CA core stability in vitro

Detergent treatment of wild-type and mutant SIV particles was performed essentially as described previously [34]. Briefly, viruses from COS-1 cells transfected with viral molecular clone DNAs (normalized by RT activity) were concentrated by ultracentrifugation at 35,000 × rpm for 75 min at 4°C in a SW41 rotor (Beckman Instruments, Tokyo, Japan) through a cushion of 20% sucrose in phosphate buffered saline (PBS). The concentrated viral pellets were suspended in PBS. Sucrose step gradients were prepared in SW55 centrifuge tubes with the 2.0 ml layer of 60% sucrose on the bottom and 2.1 ml layer of 20% sucrose overlaid. Then, 0.1 ml of Triton X-100 in PBS and 0.5 ml of concentrated viruses were overlaid and ultracentrifuged at 35,000 × rpm for 60 min at 4°C in a SW55Ti rotor (Beckman Instruments). Three fractions (top [a], middle [b], and bottom [c]) of 1.1 ml each were collected from the top and subjected to Western blot analysis using plasma from a simian-human immunodeficiency virus 89.6PD-infected rhesus macaque [55] and RT assay.

Acknowledgements

This work was supported by grants-in-aid from the Ministry of Education, Culture, Sports, Science, and Technology, a grant-in-aid from the Japan Society for the Promotion of Science, grants-in-aid from the Ministry of Health, Labor, and Welfare, and a grant from Takeda Science Foundation in Japan. NI is a Research Fellow of the Japan Society for the Promotion of Science.

Author details

[1]International Research Center for Infectious Diseases, The Institute of Medical Science, The University of Tokyo, 4-6-1 Shirokanedai, Minato-ku, Tokyo 108-8639, Japan. [2]Pathogen Genomic Center, National Institute of Infectious Diseases, 4-7-1 Gakuen, Musashimurayama, Tokyo 208-0011, Japan. [3]Department of Microbiology, Yokohama City University School of Medicine, 3-9 Fuku-ura, Kanazawa-ku, Yokohama 236-0004, Japan.

Authors' contributions

NI and TM designed the study. NI, HT, and AR performed virological analyses in vitro. MY and HS performed structure modeling analyses. HY and MK examined viral genome sequences. NI and TM analyzed the data and wrote the paper. All authors read and approved the final manuscript.

Competing interests

The authors declare that they have no competing interests.

Received: 23 August 2010 Accepted: 18 October 2010
Published: 18 October 2010

References

1. Coffin J: **HIV population dynamics in vivo: implications for genetic variation, pathogenesis, and therapy.** *Science* 1995, **267**:483-489.
2. McMichael AJ, Rowland-Jones SL: **Cellular immune responses to HIV.** *Nature* 2001, **410**:980-987.
3. Goulder PJ, Watkins DI: **HIV and SIV CTL escape: implications for vaccine design.** *Nat Rev Immunol* 2004, **4**:630-640.
4. Momany C, Kovari LC, Prongay AJ, Keller W, Gitti RK, Lee BM, Gorbalenya AE, Tong L, McClure J, Ehrlich LS, Summers MF, Carter C, Rossmann MG: **Crystal structure of dimeric HIV-1 capsid protein.** *Nat Struct Mol Biol* 1996, **3**:763-770.
5. Gamble TR, Yoo S, Vajdos FF, von Schwedler UK, Worthylake DK, Wang H, McCutcheon JP, Sundquist WI, Hill CP: **Structure of the carboxyl-terminal dimerization domain of the HIV-1 capsid protein.** *Science* 1997, **278**:849-853.
6. Berthet-Colominas C, Monaco S, Novelli A, Sibai G, Mallet F, Cusack S: **Head-to-tail dimers and interdomain flexibility revealed by the crystal structure of HIV-1 capsid protein (p24) complexed with a monoclonal antibody Fab.** *EMBO J* 1999, **18**:1124-1136.
7. Goulder PJR, Watkins DI: **Impact of MHC class I diversity on immune control of immunodeficiency virus replication.** *Nat Rev Immunol* 2008, **8**:619-630.
8. Koup RA, Safrit JT, Cao Y, Andrews CA, McLeod G, Borkowsky W, Farthing C, Ho DD: **Temporal association of cellular immune responses with the initial control of viremia in primary human immunodeficiency virus type 1 syndrome.** *J Virol* 1994, **68**:4650-4655.
9. Borrow P, Lewicki H, Hahn BH, Shaw GM, Oldstone MB: **Virus-specific CD8+ cytotoxic T-lymphocyte activity associated with control of viremia in primary human immunodeficiency virus type 1 infection.** *J Virol* 1994, **68**:6103-6110.
10. Matano T, Shibata R, Siemon C, Connors M, Lane HC, Martin MA: **Administration of an anti-CD8 monoclonal antibody interferes with the clearance of chimeric simian/human immunodeficiency virus during primary infections of rhesus macaques.** *J Virol* 1998, **72**:164-169.
11. Jin X, Bauer DE, Tuttleton SE, Lewin S, Gettie A, Blanchard J, Irwin CE, Safrit JT, Mittler J, Weinberger L, Kostrikis LG, Zhang L, Perelson AS, Ho DD: **Dramatic rise in plasma viremia after CD8+ T cell depletion in simian immunodeficiency virus-infected macaques.** *J Exp Med* 1999, **189**:991-998.
12. Schmitz JE, Kuroda MJ, Santra S, Sasseville VG, Simon MA, Lifton MA, Racz P, Tenner-Racz K, Dalesandro M, Scallon BJ, Ghrayeb J, Forman MA, Montefiori DC, Rieber EP, Letvin NL, Reimann KA: **Control of viremia in simian immunodeficiency virus infection by CD8+ lymphocytes.** *Science* 1999, **283**:857-860.
13. Phillips RE, Rowland-Jones S, Nixon DF, Gotch FM, Edwards JP, Ogunlesi AO, Elvin JG, Rothbard JA, Bangham CR, Rizza CR, McMichael AJ: **Human immunodeficiency virus genetic variation that can escape cytotoxic T cell recognition.** *Nature* 1991, **354**:453-459.
14. Borrow P, Lewicki H, Wei X, Horwitz MS, Peffer N, Meyers H, Nelson JA, Gairin JE, Hahn BH, Oldstone MB, Shaw GM: **Antiviral pressure exerted by HIV-1-specific cytotoxic T lymphocytes (CTL) during primary infection demonstrated by rapid selection of CTL escape virus.** *Nat Med* 1997, **3**:205-211.
15. Goulder PJ, Phillips RE, Colbert RA, McAdam S, Ogg G, Nowak MA, Giangrande P, Luzzi G, Morgana B, Edwards A, McMichael AJ, Rowland-Jones S: **Late escape from an immunodominant cytotoxic T-lymphocyte response associated with progression to AIDS.** *Nat Med* 1997, **3**:212-217.
16. Price DA, Goulder PJ, Klenerman P, Sewell AK, Easterbrook PJ, Troop M, Bangham CR, Phillips RE: **Positive selection of HIV-1 cytotoxic T lymphocyte escape variants during primary infection.** *Proc Natl Acad Sci USA* 1997, **94**:1890-1895.
17. Peyerl FW, Barouch DH, Yeh WW, Bazick HS, Kunstman J, Kunstman KJ, Wolinsky SM, Letvin NL: **Simian-human immunodeficiency virus escape from cytotoxic T-lymphocyte recognition at a structurally constrained epitope.** *J Virol* 2003, **77**:12572-12578.
18. Friedrich TC, Frye CA, Yant LJ, O'Connor DH, Kriewaldt NA, Benson M, Vojnov L, Dodds EJ, Cullen C, Rudersdorf R, Hughes AL, Wilson N, Watkins DI: **Extra-epitopic compensatory substitutions partially restore fitness to simian immunodeficiency virus variants that escape from an immunodominant cytotoxic T-lymphocyte response.** *J Virol* 2004, **78**:2581-2585.
19. Matano T, Kobayashi M, Igarashi H, Takeda A, Nakamura H, Kano M, Sugimoto C, Mori K, Iida A, Hirata T, Hasegawa M, Yuasa T, Miyazawa M, Takahashi Y, Yasunami M, Kimura A, O'Connor DH, Watkins DI, Nagai Y: **Cytotoxic T lymphocyte-based control of simian immunodeficiency virus**

replication in a preclinical AIDS vaccine trial. *J Exp Med* 2004, **199**:1709-1718.

20. O'Connor DH, McDermott AB, Krebs KC, Dodds EJ, Miller JE, Gonzalez EJ, Jacoby TJ, Yant L, Piontkivska H, Pantophlet R, Burton DR, Rehrauer WM, Wilson N, Hughes AL, Watkins DI: **A dominant role for CD8+-T-lymphocyte selection in simian immunodeficiency virus sequence variation.** *J Virol* 2004, **78**:14012-14022.
21. Martinez-Picado J, Prado JG, Fry EE, Pfafferott K, Leslie A, Chetty S, Thobakgale C, Honeyborne I, Crawford H, Matthews P, Pillay T, Rousseau C, Mullins JI, Brander C, Walker BD, Stuart DI, Kiepiela P, Goulder P: **Fitness cost of escape mutations in p24 Gag in association with control of human immunodeficiency virus type 1.** *J Virol* 2006, **80**:3617-3623.
22. Crawford H, Prado JG, Leslie A, Hué S, Honeyborne I, Reddy S, van der Stok M, Mncube Z, Brander C, Rousseau C, Mullins JI, Kaslow R, Goepfert P, Allen S, Hunter E, Mulenga J, Kiepiela P, Walker BD, Goulder PJR: **Compensatory mutation partially restores fitness and delays reversion of escape mutation within the immunodominant HLA-B*5703-restricted Gag epitope in chronic human immunodeficiency virus type 1 infection.** *J Virol* 2007, **81**:8346-8351.
23. Schneidewind A, Brockman MA, Yang R, Adam RI, Li B, Gall SL, Rinaldo CR, Craggs SL, Allgaier RL, Power KA, Kuntzen T, Tung CS, LaBute MX, Mueller SM, Harrer T, McMichael AJ, Goulder PJR, Aiken C, Brander C, Kelleher AD, Allen TM: **Escape from the dominant HLA-B27-restricted cytotoxic T-lymphocyte response in Gag is associated with a dramatic reduction in human immunodeficiency virus type 1 replication.** *J Virol* 2007, **81**:12382-12393.
24. Kestler HW, Ringler DJ, Mori K, Panicali DL, Sehgal PK, Daniel MD, Desrosiers RC: **Importance of the nef gene for maintenance of high virus loads and for development of AIDS.** *Cell* 1991, **65**:651-662.
25. Kawada M, Tsukamoto T, Yamamoto H, Iwamoto N, Kurihara K, Takeda A, Moriya C, Takeuchi H, Akari H, Matano T: **Gag-specific cytotoxic T lymphocyte-based control of primary simian immunodeficiency virus replication in a vaccine trial.** *J Virol* 2008, **82**:10199-10206.
26. Kobayashi M, Igarashi H, Takeda A, Kato M, Matano T: **Reversion in vivo after inoculation of a molecular proviral DNA clone of simian immunodeficiency virus with a cytotoxic-T-lymphocyte escape mutation.** *J Virol* 2005, **79**:11529-11532.
27. Hirsch V, Adger-Johnson D, Campbell B, Goldstein S, Brown C, Elkins W, Montefiori D: **A molecularly cloned, pathogenic, neutralization-resistant simian immunodeficiency virus, SIVsmE543-3.** *J Virol* 1997, **71**:1608-1620.
28. Moriya C, Igarashi H, Takeda A, Tsukamoto T, Kawada M, Yamamoto H, Inoue M, Iida A, Shu T, Hasegawa M, Nagai Y, Matano T: **Abrogation of AIDS vaccine-induced cytotoxic T lymphocyte efficacy in vivo due to a change in viral epitope flanking sequences.** *Microbes Infect* 2008, **10**:285-292.
29. Ganser BK, Li S, Klishko VY, Finch JT, Sundquist WI: **Assembly and analysis of conical models for the HIV-1 core.** *Science* 1999, **283**:80-83.
30. Li S, Hill CP, Sundquist WI, Finch JT: **Image reconstructions of helical assemblies of the HIV-1 CA protein.** *Nature* 2000, **407**:409-413.
31. Ganser-Pornillos BK, Cheng A, Yeager M: **Structure of full-length HIV-1 CA: a model for the mature capsid lattice.** *Cell* 2007, **131**:70-79.
32. Ganser-Pornillos BK, Yeager M, Sundquist WI: **The structural biology of HIV assembly.** *Curr Opin Struct Biol* 2008, **18**:203-217.
33. Pornillos O, Ganser-Pornillos BK, Kelly BN, Hua Y, Whitby FG, Stout CD, Sundquist WI, Hill CP, Yeager M: **X-Ray Structures of the hexameric building block of the HIV capsid.** *Cell* 2009, **137**:1282-1292.
34. Khan MA, Aberham C, Kao S, Akari H, Gorelick R, Bour S, Strebel K: **Human immunodeficiency virus type 1 Vif protein is packaged into the nucleoprotein complex through an interaction with viral genomic RNA.** *J Virol* 2001, **75**:7252-7265.
35. Kawada M, Igarashi H, Takeda A, Tsukamoto T, Yamamoto H, Dohki S, Takiguchi M, Matano T: **Involvement of multiple epitope-specific cytotoxic T-lymphocyte responses in vaccine-based control of simian immunodeficiency virus replication in rhesus macaques.** *J Virol* 2006, **80**:1949-1958.
36. Tsukamoto T, Takeda A, Yamamoto T, Yamamoto H, Kawada M, Matano T: **Impact of cytotoxic-T-lymphocyte memory induction without virus-specific CD4+ T-Cell help on control of a simian immunodeficiency virus challenge in rhesus macaques.** *J Virol* 2009, **83**:9339-9346.
37. Reicin A, Ohagen A, Yin L, Hoglund S, Goff S: **The role of Gag in human immunodeficiency virus type 1 virion morphogenesis and early steps of the viral life cycle.** *J Virol* 1996, **70**:8645-8652.
38. Freed EO: **HIV-1 gag proteins: diverse functions in the virus life cycle.** *Virology* 1999, **251**:1-15.
39. Lanman J, Lam TT, Barnes S, Sakalian M, Emmett MR, Marshall AG, Prevelige PE Jr: **Identification of novel interactions in HIV-1 capsid protein assembly by high-resolution mass spectrometry.** *J Mol Biol* 2003, **325**:759-772.
40. Lanman J, Lam TT, Emmett MR, Marshall AG, Sakalian M, Prevelige PE: **Key interactions in HIV-1 maturation identified by hydrogen-deuterium exchange.** *Nat Struct Mol Biol* 2004, **11**:676-677.
41. Byeon I-JL, Meng X, Jung J, Zhao G, Yang R, Ahn J, Shi J, Concel J, Aiken C, Zhang P, Gronenborn AM: **Structural convergence between Cryo-EM and NMR reveals intersubunit interactions critical for HIV-1 capsid function.** *Cell* 2009, **139**:780-790.
42. Forshey BM, von Schwedler U, Sundquist WI, Aiken C: **Formation of a human immunodeficiency virus type 1 core of optimal stability is crucial for viral replication.** *J Virol* 2002, **76**:5667-5677.
43. Sundquist WI, Hill CP: **How to assemble a capsid.** *Cell* 2007, **131**:17-19.
44. Kiepiela P, Ngumbela K, Thobakgale C, Ramduth D, Honeyborne I, Moodley E, Reddy S, de Pierres C, Mncube Z, Mkhwanazi N, Bishop K, van der Stok M, Nair K, Khan N, Crawford H, Payne R, Leslie A, Prado J, Prendergast A, Frater J, McCarthy N, Brander C, Learn GH, Nickle D, Rousseau C, Coovadia H, Mullins JI, Heckerman D, Walker BD, Goulder P: **CD8+ T-cell responses to different HIV proteins have discordant associations with viral load.** *Nat Med* 2007, **13**:46-53.
45. Sacha JB, Chung C, Rakasz EG, Spencer SP, Jonas AK, Bean AT, Lee W, Burwitz BJ, Stephany JJ, Loffredo JT, Allison DB, Adnan S, Hoji A, Wilson NA, Friedrich TC, Lifson JD, Yang OO, Watkins DI: **Gag-specific CD8+ T lymphocytes recognize infected cells before AIDS-virus integration and viral protein expression.** *J Immunol* 2007, **178**:2746-2754.
46. Willey RL, Smith DH, Lasky LA, Theodore TS, Earl PL, Moss B, Capon DJ, Martin MA: **In vitro mutagenesis identifies a region within the envelope gene of the human immunodeficiency virus that is critical for infectivity.** *J Virol* 1988, **62**:139-147.
47. Akari H, Mori K, Terao K, Otani I, Fukasawa M, Mukai R, Yoshikawa Y: **In vitro immortalization of old world monkey T lymphocytes with herpesvirus saimiri: its susceptibility to infection with simian immunodeficiency viruses.** *Virology* 1996, **218**:382-388.
48. Howard BR, Vajdos FF, Li S, Sundquist WI, Hill CP: **Structural insights into the catalytic mechanism of cyclophilin A.** *Nat Struct Mol Biol* 2003, **10**:475-481.
49. Deshpande N, Addess KJ, Bluhm WF, Merino-Ott JC, Townsend-Merino W, Zhang Q, Knezevich C, Xie L, Chen L, Feng Z, Green RK, Flippen-Anderson JL, Westbrook J, Berman HM, Bourne PE: **The RCSB Protein Data Bank: a redesigned query system and relational database based on the mmCIF schema.** *Nucleic Acids Res* 2005, **33**:D233-D237.
50. Song H, Nakayama EE, Yokoyama M, Sato H, Levy JA, Shioda T: **A single amino acid of the human immunodeficiency virus type 2 capsid affects its replication in the presence of cynomolgus monkey and human TRIM5alphas.** *J Virol* 2007, **81**:7280-7285.
51. Shirakawa K, Takaori-Kondo A, Yokoyama M, Izumi T, Matsui M, Io K, Sato T, Sato H, Uchiyama T: **Phosphorylation of APOBEC3G by protein kinase A regulates its interaction with HIV-1 Vif.** *Nat Struct Mol Biol* 2008, **15**:1184-1191.
52. Labute P: **The generalized Born/volume integral implicit solvent model: estimation of the free energy of hydration using London dispersion instead of atomic surface area.** *J Comp Chem* 2008, **29**:1693-1698.
53. Ponder JW, Case DA: **Force fields for protein simulations.** *Adv Protein Chem* 2003, **66**:27-85.
54. Onufriev A, Bashford D, Case DA: **Modification of the generalized Born model suitable for macromolecules.** *J Phys Chem B* 2000, **104**:3712-3720.
55. Matano T, Kano M, Nakamura H, Takeda A, Nagai Y: **Rapid appearance of secondary immune responses and protection from acute CD4 depletion after a highly pathogenic immunodeficiency virus challenge in macaques vaccinated with a DNA prime/Sendai virus vector boost regimen.** *J Virol* 2001, **75**:11891-11896.

doi:10.1186/1742-4690-7-90
Cite this article as: Inagaki *et al.*: **A structural constraint for functional interaction between N-terminal and C-terminal domains in simian immunodeficiency virus capsid proteins.** *Retrovirology* 2010 **7**:90.

ELSEVIER

INSTITUT PASTEUR

Microbes and Infection 13 (2011) 58–64

www.elsevier.com/locate/micinf

Original article

Improved capacity of a monkey-tropic HIV-1 derivative to replicate in cynomolgus monkeys with minimal modifications

Akatsuki Saito [a,b,c,1], Masako Nomaguchi [d,1], Sayuki Iijima [c], Ayumu Kuroishi [e], Tomoyuki Yoshida [b], Young-Jung Lee [c], Toshiyuki Hayakawa [b], Ken Kono [e], Emi E. Nakayama [e], Tatsuo Shioda [e], Yasuhiro Yasutomi [c], Akio Adachi [d], Tetsuro Matano [a], Hirofumi Akari [b,c,*]

[a] *International Research Center for Infectious Diseases, The Institute of Medical Science, The University of Tokyo, Tokyo 108-8639, Japan*
[b] *Primate Research Institute, Kyoto University, Inuyama 484-8506, Japan*
[c] *Tsukuba Primate Research Center, National Institute of Biomedical Innovation, Tsukuba 305-0843, Japan*
[d] *Department of Microbiology, Institute of Health Biosciences, The University of Tokushima Graduate School, Tokushima 770-8503, Japan*
[e] *Department of Viral Infections, Research Institute for Microbial Diseases, Osaka University, Suita 565-0871, Japan*

Received 31 July 2010; accepted 1 October 2010
Available online 16 October 2010

Abstract

Human immunodeficiency virus type 1 (HIV-1) hardly replicates in Old World monkeys. Recently, a mutant HIV-1 clone, NL-DT5R, in which a small part of *gag* and the entire *vif* gene are replaced with SIVmac239-derived ones, was shown to be able to replicate in pigtail monkeys but not in rhesus monkeys (RM). In the present study, we found that a modified monkey-tropic HIV-1 (HIV-1mt), MN4-5S, acquired the ability to replicate efficiently in cynomolgus monkeys as compared with the NL-DT5R, while neither NL-DT5R nor MN4-5S replicated in RM cells. These results suggest that multiple determinants may be involved in the restriction of HIV-1 replication in macaques, depending on the species of macaques. The new HIV-1mt clone will be useful for studying molecular mechanisms by which anti-viral host factors regulate HIV-1 replication in macaques.

Keywords: HIV-1; Old World monkey; TRIM5α

1. Introduction

Human immunodeficiency virus type 1 (HIV-1) productively infects only humans but not Old World monkeys (OWM) such as cynomolgus monkeys (CM) or rhesus monkeys (RM), whereas RM-derived simian immunodeficiency virus (SIVmac) can efficiently replicate in OWM. Because of this species barrier, alternative monkey models using SIVmac or simian/human immunodeficiency viruses (SHIV) have been used for AIDS research [1–4]. However, detailed analyses of molecular mechanisms of the pathogenesis of HIV-1 have been hampered by the lack of appropriate non-human primate models for HIV-1 infection.

The mechanistic basis for the inability of HIV-1 to replicate in OWM cells has remained unclear. Recently, a number of intrinsic anti-HIV-1 cellular factors, including tripartite motif protein 5α (TRIM5α), Cyclophilin A (CypA), apolipoprotein B mRNA-editing catalytic polypeptide (APOBEC3) family and Tetherin were discovered in OWM cells [5,6]. TRIM5α strongly suppresses HIV-1 replication, mainly by affecting the viral disassembly step, resulting in a decrease of reverse transcription products [7,8]. CypA acts as a regulator promoting TRIM5α-mediated restriction of HIV-1 [8]. APOBEC3 is also a major regulator of HIV-1 replication [9,10]. APOBEC3 exerts its inhibitory effect mainly by inducing G to A hypermutation

* Corresponding author. Primate Research Institute, Kyoto University, Inuyama 484-8506, Japan. Tel.: +81 568 63 0440; fax: +81 568 63 0459.
E-mail address: akari@pri.kyoto-u.ac.jp (H. Akari).
[1] A.S. and M.N. contributed equally to this work.

1286-4579/$ - see front matter © 2010 Institut Pasteur. Published by Elsevier Masson SAS. All rights reserved.
doi:10.1016/j.micinf.2010.10.001

into the viral genome due to its cytidine deaminase activity, while hypermutation-independent inhibitory activity at the stage of reverse transcription is also evident [11]. Tetherin, also referred to as a BST-2, was identified as an intrinsic anti-viral factor that restricts the egress of HIV-1 by tethering virions to the host cell surface [12,13]. Importantly, HIV-1 can counteract human APOBEC3 activity by utilizing the viral accessory protein Vif, whereas it cannot counteract OWM APOBEC3 [14]. Similarly, HIV-1 counteracts human Tetherin activity by utilizing another viral accessory protein Vpu, whereas HIV-1 does not counteract OWM Tetherin activity [15].

In an attempt to generate a monkey-tropic HIV-1 (HIV-1mt), Kamada et al. constructed an HIV-1 variant carrying minimal SIVmac-derived sequences to overcome the restriction factors [16]. The prototype HIV-1 clone NL-DT5R had a sequence encoding an SIVmac loop between alpha helices 4 and 5 (L4/5) of *capsid* gene (CA) and the entire *vif* gene, which relieved the inhibitory effects on viral replication by restriction factors CypA, TRIM5α and APOBEC3. NL-DT5R was able to replicate in pigtail monkeys (PM) in vivo as well as in vitro, as reported by Igarashi et al. [17]. Although NL-DT5R induced immune responses in infected animals, the virus did not establish persistent infection.

In the present study, we sought to adapt NL-DT5R to CM by performing long-term passage in CM-derived HSC-F cells. We successfully obtained a modified HIV-1mt clone having several mutations. Additionally, we inserted an SIVmac loop between alpha helices 6 and 7 (L6/7) of CA [18]. The resultant clone named MN4-5S was found to replicate efficiently and to induce strong immune responses in infected CM, suggesting the impact of viral adaptation.

2. Materials and methods

2.1. Plasmid construction

The HIV-1 derivatives were constructed on a background of an infectious molecular clone, NL4-3 [19]. NL-DT5R, a cloned virus containing SIVmac239 L4/5 and the entire *vif* gene, was reported previously by Kamada et al. [16]. In addition, NL-DT562, a virus having an R5-tropic SF162-derived *env* gene on a background of NL-DT5R, was used in this study [20]. After long passage of NL-DT5R and NL-DT562 in cynomolgus T cell line HSC-F [21], several mutations were appeared in both viral genomes, and then all of them were inserted into NL-DT5R by gene-engineering techniques. Consequently, a clone having 14 nucleotide substitutions in its genome was constructed and named MN4-5. Among these substitutions, 7 were non-synonymous mutations. The structure of the clone is shown in Fig. 1. A part of L6/7 of CA (aa residues 120–122; HNP) of MN4-5 was also replaced with the corresponding segment of SIVmac239 CA (aa residues 120–123; RQQN) by means of site-directed mutagenesis as described previously in Ref. [18]. The resultant construct was designated MN4-5S.

2.2. Cells and viruses

Human embryonic kidney cell line HEK293T was maintained in DMEM supplemented with 10% fetal bovine serum, 100 units/ml of penicillin and 100 μg/ml of streptomycin (Sigma). Monkey peripheral blood mononuclear cells (PBMCs) were separated with a standard Ficoll density gradient separation method and cultured in R-10 composed of

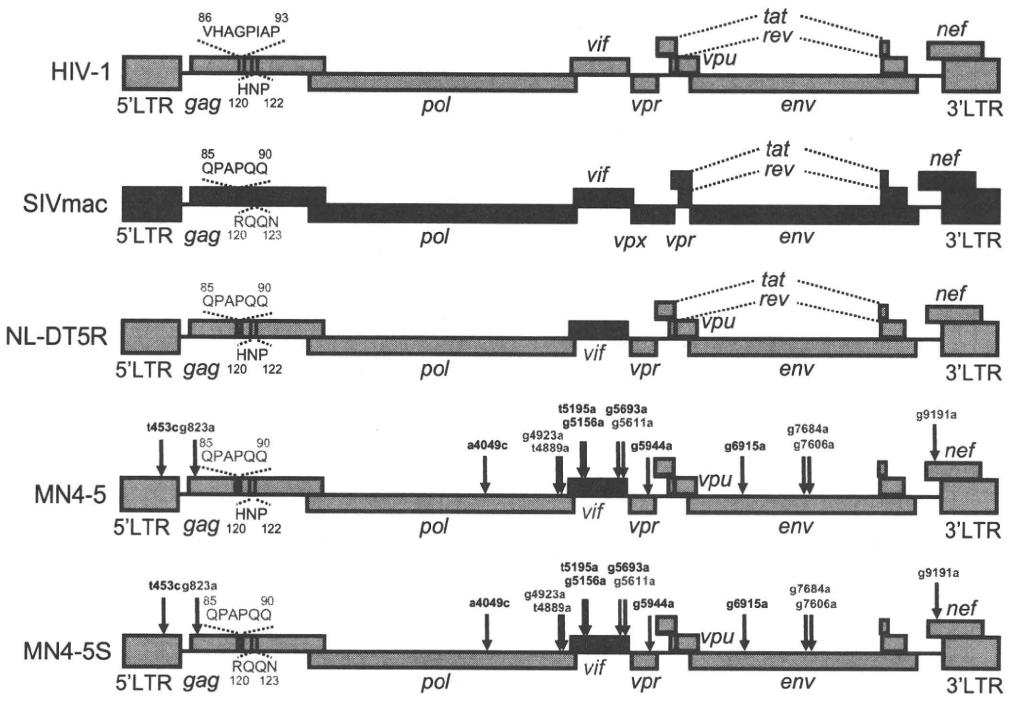

Fig. 1. Structure of HIV-1mt clones used in this study. The positions of nucleotide mutations are indicated by arrows in this figure. Among nucleotide substitutions, the positions of non-synonymous mutations are indicated in red.

RPMI-1640 medium supplemented with 10% fetal bovine serum, 100 units/ml of penicillin and 100 μg/ml of streptomycin (Sigma). The growth kinetics of each HIV-1 clone were examined in activated $CD8^+$ cell-depleted PBMCs. Briefly, separated PBMCs were reacted with a PE-labeled anti-CD8 antibody and then treated with anti-PE magnetic beads. After washing, $CD8^+$ cell-depleted PBMCs were negatively separated by using MACS columns (Miltenyi Biotec). For stimulation, $CD8^+$ cell-depleted PBMCs were first cultured in R-10 containing 1 μg/ml of concanavalin A (Sigma) for 2 days followed by culture in R-10 supplemented with 100 U/ml IL-2 (Shionogi) for more 2 days. The cells were then infected with 100 ng of p24 of HIV-1 and the culture supernatant was collected periodically. HSC-F, a cynomolgus monkey-derived $CD4^+$ T cell line [21], was cultured in R-10.

Virus stocks were prepared as follows: sub-confluent HEK293T cells were transfected with proviral DNA using Lipofectamine2000 reagent according to the manufacturer's instructions. At 42 h after transfection, culture supernatants were centrifuged, filtrated with a 0.45 μm filter, and aliquoted as virus stocks for in vitro experiments. For preparation of viral stocks for in vivo experiments, $CD8^+$ cell-depleted PBMCs were infected with the HEK293T-derived stocks as described above. After washing, the cells were maintained for several days and the culture supernatants were collected and stored as described above.

2.3. Reverse transcription (RT) assay

Virion-associated RT activity was measured as described previously in Ref. [22]. HSC-F cells (1×10^6) were infected with equal amounts of viruses (1×10^7 RT units). Viral growth kinetics was determined by RT production in the culture supernatants.

2.4. Animal experiments

Healthy adult cynomolgus monkeys were used in this study. All animals were confirmed to be negative for simian retrovirus and were housed in individual isolators in a biosafety level 3 facility and maintained according to the National Institute of Biomedical Innovation rules and guidelines for experimental animal welfare. Bleeding and viral inoculation were performed under ketamine hydrochloride anesthesia. Viral stocks for inoculation were inoculated into each animal. The profiles of plasma viral RNA loads, circulating $CD4^+$ and $CD8^+$ T lymphocytes were evaluated as described below.

2.5. Flow cytometry and immunophenotyping of peripheral blood lymphocytes

Immunophenotyping of freshly isolated PBMCs was performed according to standard procedures using multicolor flow cytometry performed with a FACSCantoII (Becton Dickinson). $CD4^+$ and $CD8^+$ T cells were identified using monoclonal antibodies (mAbs) to CD3 (clone SP34-2, BD Pharmingen), CD4 (clone L200, BD Pharmingen) and CD8 (clone DK25, DAKO). Flow cytometric acquisition and analysis of samples was performed on at least 10,000 events collected by a flow cytometer driven by FACSDiVa software.

2.6. Analysis of anti-viral antibody response

Plasma samples from infected animals were first heat-inactivated at 56 °C for 30 min. Then, 100-fold diluted samples were reacted with commercially available anti-HIV-1 antibody detection strips (New LAV Blot I, Bio-Rad) according to the manufacture's instructions.

2.7. In vivo depletion of $CD8^+$ lymphocytes

Infected animals received an anti-CD8 mAb (cM-T807) as follows: 10 mg/kg (body weight) inoculation subcutaneously at 42 days post infection (DPI), followed by 5 mg/kg inoculation intravenously at 45, 49, and 52 DPI. The cM-T807 mAb was provided by the NIH Nonhuman Primate Reagent Resource. To repeatedly confirm the depletion of $CD8^+$ cells in the presence of cM-T807, an anti-CD8 mAb (clone DK25, DAKO) was used as reported previously in Ref. [23].

2.8. Quantification of viral RNA

Total RNA was collected from monkey plasma using a High Pure Viral RNA Kit (Roche Diagnostics) according to the manufacturer's instructions. Viral RNA was quantified with a quantitative real-time PCR system using TaqMan One-Step RT-PCR Master Mix Reagents (Applied Biosystems). The primers and probe used in this study were as follows: Forward primer: HIVgag683 (+) (5′-CTCTCGACGCAGGACTCGGCTTGCT-3′); Reverse primer: HIVgag803 (−) (5′-GCTCTCGCACCCATCTCTCTCCTTCTAGCC-3′); Probe: HIVgag TaqMan 720R748 (FAM-GCAAGAGGCGAGRGGCGGCGACTGGTGAG-TAMRA). The quantification and data analysis were performed using the iQ5 Real-Time PCR Detection System (Bio-Rad). The detection limit of this assay was 400-copies/ml plasma.

3. Results

3.1. Growth properties of prototype HIV-1mt clone, NL-DT5R in macaques in vitro and in vivo

We first examined the replication properties of prototype HIV-1mt NL-DT5R in $CD8^+$ cell-depleted PBMCs of CM and RM. NL-DT5R replicated in the cells of CM but not in those of RM (Fig. 2). We next examined the in vivo replication properties of NL-DT5R in CM. Viral stocks for inoculation were prepared with $CD8^+$ cell-depleted CM PBMCs as described above. Then, two monkeys were infected with NL-DT5R intravenously and bled periodically. As shown in Fig. 3A, NL-DT5R established infection as indicated by detectable levels of plasma viremia and an anti-HIV-1 antibody response, although the viral level was marginal (about 1×10^3 copies/ml) and disappeared at 4 weeks post infection.

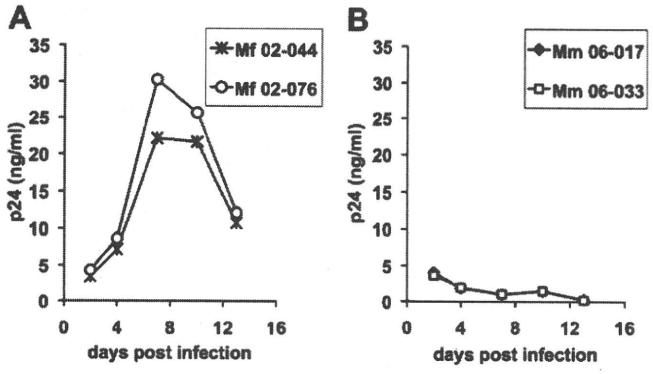

Fig. 2. Growth properties of the NL-DT5R in $CD8^+$ cell-depleted PBMCs from CM (A) and RM (B). The cells were infected with NL-DT5R and the viral replication was monitored by p24 antigen in the culture supernatants using a p24 quantitative ELISA kit. Animal identifications are indicated at the top of each panel.

These results indicated that although CM appeared permissive for NL-DT5R as compared with RM, the mutations introduced in NL-DT5R were not still sufficient to overcome the restriction by host factor(s) of these macaques.

3.2. MN4-5S showed improved replication capability in CM $CD8^+$ cell-depleted PBMCs

In order to improve the replication capability of HIV-1mt in CM, we conducted long-term passage of NL-DT5R in HSC-F cells. Additionally, NL-DT562, having an R5-tropic *env* gene on a background of NL-DT5R, was also passaged long-term in HSC-F cells. We found that the passaging improved the growth of the viruses (data not shown), and then viral clones were obtained after the long-term passaging and sequenced. Ten nucleotide substitutions were identified in the NL-DT5R-derived clone and 4 nucleotide substitutions (except for the *env* gene) in the NL-DT562-derived clone. These 14 nucleotide substitutions (7 of which were non-synonymous mutations) were assembled and introduced into NL-DT5R. The resultant clone was named MN4-5, and its structure is shown in Fig. 1. We previously found that insertion of an SIVmac loop between alpha helices 6 and 7 (L6/7) of CA into the corresponding region in HIV-1 significantly enhanced the viral replication in HSC-F cells and PBMCs of CM by relieving the inhibitory effect of TRIM5α [18]. We therefore inserted an SIVmac-derived L6/7 sequence into MN4-5. The resultant clone was named MN4-5S (Fig. 1). In order to examine the impact of these modifications on the viral replication, we analyzed the replication properties of this "adapted" virus in HSC-F cells and $CD8^+$ cell-depleted PBMCs of CM. MN4-5 showed higher replication as compared with NL-DT5R in both types of cells (Figs. 4 and 5). Moreover, MN4-5S showed enhanced growth capability in the cells as compared with the parental clones, NL-DT5R and MN4-5 (Figs. 4 and 5).

Notably, MN4-5S did not show any replication in RM cells (data not shown), indicating that the combination of the mutations introduced in NL-DT5R may be effective for escape from the restriction in CM cells but not in RM cells.

3.3. MN4-5S induced greater viremia in CM as compared with parental clone, NL-DT5R

Since MN4-5S showed enhanced ability to replicate in CM cells, we next examined the viral replication in vivo. The stock of MN4-5S virus was inoculated into 3 CM. MN4-5S induced 10-fold higher viremia in infected animals at 2–3 weeks after infection (Fig. 6A), as compared with that induced by NL-DT5R (see Fig. 3). This result was consistent with the in vitro result (Fig. 5) and demonstrated that the mutations inserted into NL-DT5R contributed to enhancement of viral replication in vivo. In addition, at the acute phase of infection a slight decrease of $CD4^+$ T cells was observed (Fig. 6B). The viremia became undetectable at 6 weeks after infection.

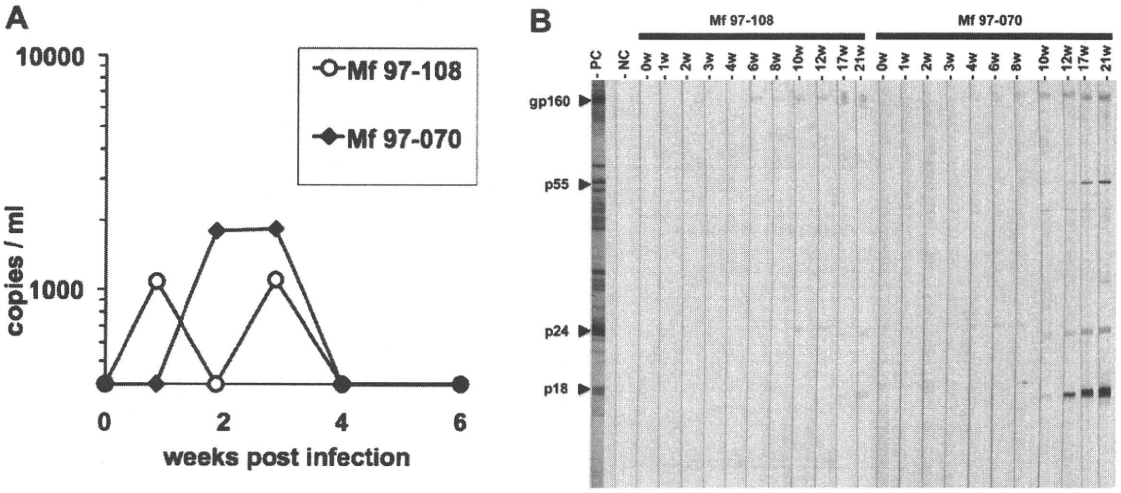

Fig. 3. Profiles of plasma viral RNA loads (A) and anti-HIV-1 antibody responses (B) in CM infected with NL-DT5R. Mf97-108 (open circles) and Mf97-070 (closed diamonds) were used in this study. Viral stocks for inoculation were prepared in $CD8^+$ cell-depleted PBMCs, and then 6.1 ng p24 of HIV-1 were inoculated into each animal. Commercially available diagnostic HIV-1 Western blotting strips were reacted with 100-fold diluted monkey plasma. Plasma from HIV-1-infected or uninfected individuals was used as a positive or a negative control, respectively.

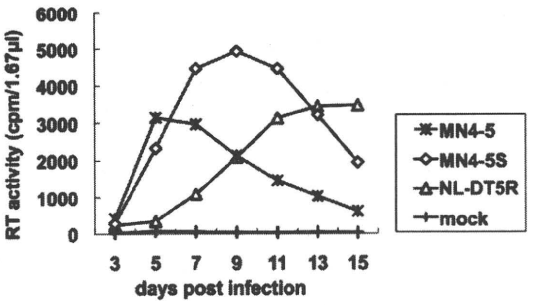

Fig. 4. Growth properties of HIV-1mt in HSC-F cells. The cells were infected with a series of HIV-1mt derivatives. The viral replication was monitored by RT activity in the culture supernatants.

Thereafter, antibody response against MN4-5S was observed in infected animals (Fig. 6C). As indicated by comparison with the lane of the positive control as a standard, the degree of antibody response seemed to be stronger than that against NL-DT5R (see Figs. 3B and 6C). Next we attempted to clarify the role of $CD8^+$ lymphocytes in the disappearance of viremia. We conducted in vivo depletion of $CD8^+$ cells by using a method reported previously [23]. We found that the reappearance of viremia was observed in all monkeys tested in parallel with the decline of $CD8^+$ T cells after the anti-CD8 mAb administration (Fig. 6A and D). This result indicated that $CD8^+$ T cells had a critical role in the control of HIV-1mt replication and suggested that the virus was able to infect latently in vivo.

4. Discussion

In the present study, we found that a modified HIV-1mt, MN4-5S, acquired greater ability to replicate in CM than NL-DT5R, and that both the SIVmac-derived L6/7 (HNP120-122 > RQQN120-123 of CA) and a series of substitutions identified by long-term passage of NL-DT5R in HSC-F cells contributed to this ability (Fig. 1). We recently showed that the substitution of L6/7 relieved the inhibitory effect of TRIM5α [18]. Additionally, our preliminary data suggest that non-synonymous mutations in the *integrase* and *env* genes are likely to be critical for the improved activity (Nomaguchi et al., manuscript in preparation). It is possible that these adaptive mutations may optimize the interaction between host and viral proteins.

It seemed that the growth kinetics of NL-DT5R in PM were comparable with those of MN4-5S in CM, which had peak levels in acute viremia of approximately 10^4 copies/ml [17]. It is therefore likely that PM may exhibit better susceptibility to HIV-1mt than CM. It is possible that the greater susceptibility of PM to HIV-1mt replication could be due to the genotype of TRIM5, because PM usually expresses a chimera between TRIM5α and CypA, so-called TRIM-Cyp, whose anti-HIV-1 activity is defective [24].

One unexpected finding in this study was that MN4-5S was unable to replicate in PBMCs of RM (data not shown), which was in contrast with the greater susceptibility of RM to SIVmac infection. Our results suggested that RM was most resistant to HIV-1mt replication among the three macaque species. Since our HIV-1mt clones (NL-DT5R and MN4-5) were established on the basis of information obtained from serial passages of the viruses in CM-derived cells, it may be reasonable to consider that these viruses were consequently optimized to CM. Alternatively, it is also possible that anti-HIV-1 activities such as TRIM5α and APOBEC3 of RM could be greater than those of other macaques. Further studies are in progress to address these questions.

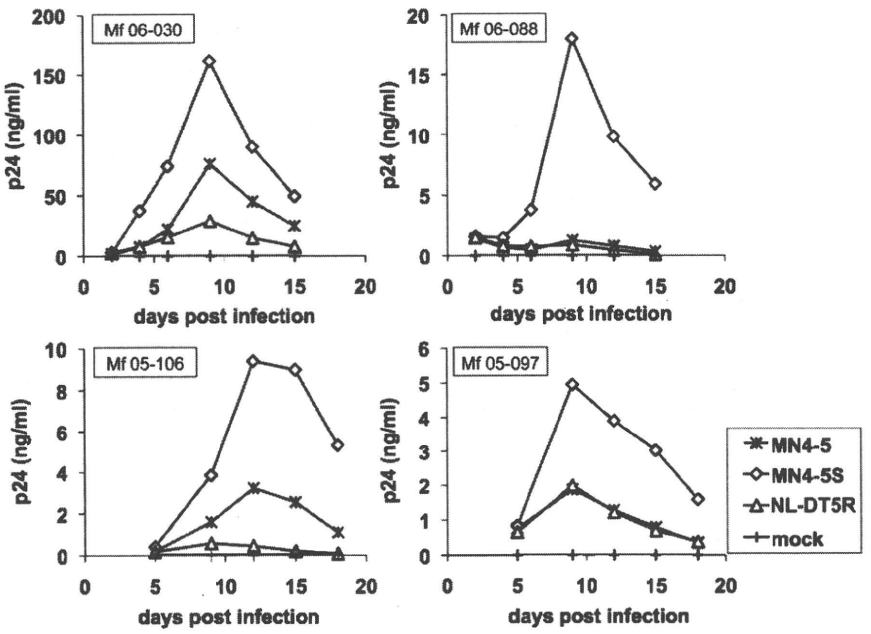

Fig. 5. Growth properties of HIV-1mt in $CD8^+$ cell-depleted PBMCs from four CM. The cells were infected with a series of HIV-1mt derivatives. The viral replication was monitored by p24 antigen in the culture supernatants using a p24 quantitative ELISA kit. Animal identifications are indicated at the top of each panel.

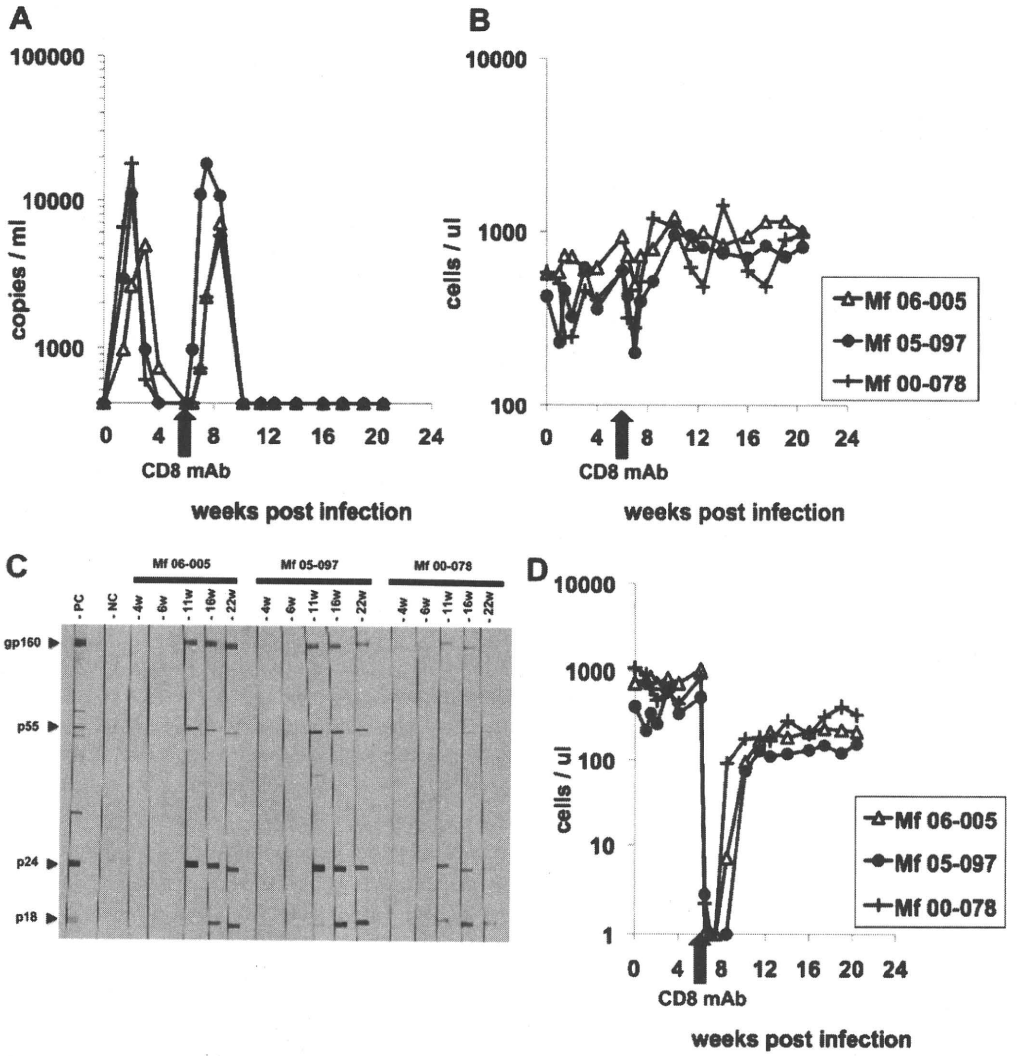

Fig. 6. Profiles of plasma viral RNA loads (A), circulating $CD4^+$ T lymphocytes (B), anti-HIV-1 antibody responses (C) and circulating $CD8^+$ T lymphocytes (D) in CM infected with HIV-1 derivatives. Viral stocks for inoculation were prepared in $CD8^+$ cell-depleted PBMCs and then 10 ng of p24 of HIV-1 were inoculated into each animal. Commercially available diagnostic HIV-1 Western blotting strips were reacted with 100-fold diluted plasma of each monkey. Plasma from HIV-1 infected or uninfected individuals was used as a positive or negative control, respectively. The black arrow indicates the day of anti-CD8 mAb (cM-T807) inoculation.

We demonstrated that the reappearance of viremia was observed in all monkeys tested in parallel with decline of $CD8^+$ T cells after anti-CD8 mAb administration (Fig. 6A and D). This result indicated that HIV-1-specific $CD8^+$ T cells had a critical role in the control of HIV-1mt replication and suggested that the virus may be able to infect latently in vivo. In order to establish a set point viremia and persistent infection, further modifications of HIV-1mt may be required to enable potent escape from the anti-viral immune response.

Further mechanistic characterization of anti-HIV-1 restriction factors will help in the construction of highly replicative and pathogenic HIV-1mt clones. As in the case of SHIV, in vivo passage of the virus could be a conventional and straightforward procedure for achieving such purposes [4]. However, the results of our study demonstrate that selective modification of HIV-1mt based on available knowledge regarding the molecular machineries is an alternative and powerful way. We are now in the process of developing the next generation of HIV-1mt that will acquire growth ability and pathogenicity in macaques as well as in humans.

Acknowledgements

The authors wish to thank T. Kurosawa, M. Fujita and M. Yasue for their helpful assistance. The authors also thank F. Ono, Y. Katakai, K. Komatsuzaki, A. Hiyaoka, K. Ohto, H. Ohto, and Y. Emoto for their support in animal experiments. We also thank M. Kaizu for his technical support. The anti-CD8 antibody used in the present study was provided by the NIH Nonhuman Primate Reagent Resource (R24 RR016001, N01 AI040101). This work was supported by grants from the Japan Health Sciences Foundation and the Ministry of Health, Labor, and Welfare in Japan and by Global COE Program A06 of Kyoto University.

References

[1] N.L. Letvin, M.D. Daniel, P.K. Sehgal, R.C. Desrosiers, R.D. Hunt, L.M. Waldron, J.J. MacKey, D.K. Schmidt, L.V. Chalifoux, N.W. King, Induction of AIDS-like disease in macaque monkeys with T-cell tropic retrovirus STLV-III, Science 230 (1985) 71–73.

[2] H. Kestler, T. Kodama, D. Ringler, M. Marthas, N. Pedersen, A. Lackner, D. Regier, P. Sehgal, M. Daniel, N. King, et al., Induction of AIDS in rhesus monkeys by molecularly cloned simian immunodeficiency virus, Science 248 (1990) 1109–1112.

[3] R. Shibata, M. Kawamura, H. Sakai, M. Hayami, A. Ishimoto, A. Adachi, Generation of a chimeric human and simian immunodeficiency virus infectious to monkey peripheral blood mononuclear cells, J. Virol. 65 (1991) 3514–3520.

[4] K.A. Reimann, J.T. Li, R. Veazey, M. Halloran, I.W. Park, G.B. Karlsson, J. Sodroski, N.L. Letvin, A chimeric simian/human immunodeficiency virus expressing a primary patient human immunodeficiency virus type 1 isolate env causes an AIDS-like disease after in vivo passage in rhesus monkeys, J. Virol. 70 (1996) 6922–6928.

[5] M. Nomaguchi, N. Doi, K. Kamada, A. Adachi, Species barrier of HIV-1 and its jumping by virus engineering, Rev. Med. Virol. 18 (2008) 261–275.

[6] D. Sauter, A. Specht, F. Kirchhoff, Tetherin: holding on and letting go, Cell 141 (2010) 392–398.

[7] M. Stremlau, C.M. Owens, M.J. Perron, M. Kiessling, P. Autissier, J. Sodroski, The cytoplasmic body component TRIM5alpha restricts HIV-1 infection in Old World monkeys, Nature 427 (2004) 848–853.

[8] E.E. Nakayama, T. Shioda, Anti-retroviral activity of TRIM5 alpha, Rev. Med. Virol. 20 (2010) 77–92.

[9] A.M. Sheehy, N.C. Gaddis, J.D. Choi, M.H. Malim, Isolation of a human gene that inhibits HIV-1 infection and is suppressed by the viral Vif protein, Nature 418 (2002) 646–650.

[10] S. Henriet, G. Mercenne, S. Bernacchi, J.C. Paillart, R. Marquet, Tumultuous relationship between the human immunodeficiency virus type 1 viral infectivity factor (Vif) and the human APOBEC-3G and APOBEC-3F restriction factors, Microbiol. Mol. Biol. Rev. 73 (2009) 211–232.

[11] M.H. Malim, APOBEC proteins and intrinsic resistance to HIV-1 infection, Philos. Trans. R Soc. Lond B. Biol. Sci. 364 (2009) 675–687.

[12] S.J. Neil, T. Zang, P.D. Bieniasz, Tetherin inhibits retrovirus release and is antagonized by HIV-1 Vpu, Nature 451 (2008) 425–430.

[13] J.L. Douglas, J.K. Gustin, K. Viswanathan, M. Mansouri, A.V. Moses, K. Fruh, The great escape: viral strategies to counter BST-2/tetherin, PLoS Pathog. 6 (2010) e1000913.

[14] R. Mariani, D. Chen, B. Schrofelbauer, F. Navarro, R. Konig, B. Bollman, C. Munk, H. Nymark-McMahon, N.R. Landau, Species-specific exclusion of APOBEC3G from HIV-1 virions by Vif, Cell 114 (2003) 21–31.

[15] B. Jia, R. Serra-Moreno, W. Neidermyer, A. Rahmberg, J. Mackey, I.B. Fofana, W.E. Johnson, S. Westmoreland, D.T. Evans, Species-specific activity of SIV Nef and HIV-1 Vpu in overcoming restriction by tetherin/BST2, PLoS Pathog. 5 (2009) e1000429.

[16] K. Kamada, T. Igarashi, M.A. Martin, B. Khamsri, K. Hatcho, T. Yamashita, M. Fujita, T. Uchiyama, A. Adachi, Generation of HIV-1 derivatives that productively infect macaque monkey lymphoid cells, Proc Natl Acad Sci U S A 103 (2006) 16959–16964.

[17] T. Igarashi, R. Iyengar, R.A. Byrum, A. Buckler-White, R.L. Dewar, C. E. Buckler, H.C. Lane, K. Kamada, A. Adachi, M.A. Martin, Human immunodeficiency virus type 1 derivative with 7% simian immunodeficiency virus genetic content is able to establish infections in pig-tailed macaques, J. Virol. 81 (2007) 11549–11552.

[18] A. Kuroishi, A. Saito, Y. Shingai, T. Shioda, M. Nomaguchi, A. Adachi, H. Akari, E.E. Nakayama, Modification of a loop sequence between alpha-helices 6 and 7 of virus capsid (CA) protein in a human immunodeficiency virus type 1 (HIV-1) derivative that has simian immunodeficiency virus (SIVmac239) vif and CA alpha-helices 4 and 5 loop improves replication in cynomolgus monkey cells, Retrovirology 6 (2009) 70.

[19] A. Adachi, H.E. Gendelman, S. Koenig, T. Folks, R. Willey, A. Rabson, M.A. Martin, Production of acquired immunodeficiency syndrome-associated retrovirus in human and nonhuman cells transfected with an infectious molecular clone, J. Virol. 59 (1986) 284–291.

[20] T. Yamashita, N. Doi, A. Adachi, M. Nomaguchi, Growth ability in simian cells of monkey cell-tropic HIV-1 is greatly affected by downstream region of the vif gene, J. Med. Invest. 55 (2008) 236–240.

[21] H. Akari, K.H. Nam, K. Mori, I. Otani, H. Shibata, A. Adachi, K. Terao, Y. Yoshikawa, Effects of SIVmac infection on peripheral blood CD4+CD8+ T lymphocytes in cynomolgus macaques, Clin. Immunol. 91 (1999) 321–329.

[22] R.L. Willey, D.H. Smith, L.A. Lasky, T.S. Theodore, P.L. Earl, B. Moss, D.J. Capon, M.A. Martin, In vitro mutagenesis identifies a region within the envelope gene of the human immunodeficiency virus that is critical for infectivity, J. Virol. 62 (1988) 139–147.

[23] J.E. Schmitz, M.A. Simon, M.J. Kuroda, M.A. Lifton, M.W. Ollert, C.W. Vogel, P. Racz, K. Tenner-Racz, B.J. Scallon, M. Dalesandro, J. Ghrayeb, E.P. Rieber, V.G. Sasseville, K.A. Reimann, A nonhuman primate model for the selective elimination of CD8+ lymphocytes using a mouse-human chimeric monoclonal antibody, Am. J. Pathol. 154 (1999) 1923–1932.

[24] C.A. Virgen, Z. Kratovac, P.D. Bieniasz, T. Hatziioannou, Independent genesis of chimeric TRIM5-cyclophilin proteins in two primate species, Proc. Natl. Acad. Sci. U S A 105 (2008) 3563–3568.

JOURNAL OF VIROLOGY, Jan. 2011, p. 1117–1124 Vol. 85, No. 2
0022-538X/11/$12.00 doi:10.1128/JVI.00657-10

Spatial Configuration of Hepatitis E Virus Antigenic Domain▽

Li Xing,[1,2]† Joseph C. Wang,[1]† Tian-Cheng Li,[3] Yasuhiro Yasutomi,[4] James Lara,[5] Yury Khudyakov,[5] Darren Schofield,[6] Suzanne U. Emerson,[6] Robert H. Purcell,[6] Naokazu Takeda,[3] Tatsuo Miyamura,[3] and R. Holland Cheng[1]*

Molecular and Cellular Biology, University of California, Davis, California 95616[1]; Karolinska Institute Structural Virology, F68 University Hospital, SE-14186 Stockholm, Sweden[2]; Department of Virology II, National Institute of Infectious Disease, Tokyo 162, Japan[3]; Tsukuba Primate Research Center, National Institute of Biomedical Innovation, Ibaraki 305-0843, Japan[4]; Division of Viral Hepatitis, Centers for Disease Control and Prevention (CDC), Atlanta, Georgia 30333[5]; and Hepatitis Virus Section, National Institute of Allergy and Infectious Diseases, Bethesda, Maryland 208892[6]

Received 26 March 2010/Accepted 28 October 2010

Hepatitis E virus (HEV) is a human pathogen that causes acute hepatitis. When an HEV capsid protein containing a 52-amino-acid deletion at the C terminus and a 111-amino-acid deletion at the N terminus is expressed in insect cells, the recombinant HEV capsid protein can self-assemble into a T=1 virus-like particle (VLP) that retains the antigenicity of the native HEV virion. In this study, we used cryoelectron microscopy and image reconstruction to show that anti-HEV monoclonal antibodies bind to the protruding domain of the capsid protein at the lateral side of the spikes. Molecular docking of the HEV VLP crystal structure revealed that Fab224 covered three surface loops of the recombinant truncated second open reading frame (ORF2) protein (PORF2) at the top part of the spike. We also determined the structure of a chimeric HEV VLP and located the inserted B-cell tag, an epitope of 11 amino acids coupled to the C-terminal end of the recombinant ORF2 protein. The binding site of Fab224 appeared to be distinct from the location of the inserted B-cell tag, suggesting that the chimeric VLP could elicit immunity against both HEV and an inserted foreign epitope. Therefore, the T=1 HEV VLP is a novel delivery system for displaying foreign epitopes at the VLP surface in order to induce antibodies against both HEV and the inserted epitope.

Hepatitis E virus (HEV) is a causative agent of acute hepatitis in humans and is primarily transmitted via the fecal-oral route. HEV is thus resistant to the low pH and digestive enzymes associated with the stomach and gastrointestinal tract. HEV regularly causes epidemics in many tropical and subtropical countries. In India, 101 outbreaks were confirmed by serological analysis in the state of Maharashtra in the last 5 years (6), and the lifetime risk of HEV infection exceeds 60% (28). Sporadic cases have also been reported in regions where HEV is endemic, as well as in areas where it is not endemic. Although some of these cases were associated with travel, many cases involved patients without a history of travel to regions where HEV is endemic. Accumulating evidence suggests that sporadic infection occurs through a zoonotic route and is not limited to developing countries. Seroprevalence suggests hepatitis E infection may also be prevalent in high-income countries (21), such as the United States (17), the United Kingdom (3), and Japan (18). The overall mortality rate of HEV infection during an outbreak generally ranges from 1 to 15%, and the highest mortality occurs in pregnant women, with fatality rates of up to 30% (19).

The HEV virion is composed of a 7.2-kb single-stranded RNA molecule and a 32- to 34-nm icosahedral capsid. The HEV genome contains three open reading frames (ORFs). The capsid protein, encoded by the second open reading frame (ORF2), located at the 3′ terminus of the genome, comprises 660 amino acids and is responsible for most capsid-related functions, such as assembly, host interaction, and immunogenicity. Recombinant ORF2 proteins can induce antibodies that block HEV infection in nonhuman primates (12, 27). Four major antigenic domains were predicted to be located within the C-terminal 268 amino acids of the ORF2 protein; one domain was experimentally identified as a neutralization epitope in the Sar-55 ORF2 capsid protein (25, 26). However, the minimal peptide needed to induce anti-HEV neutralizing antibodies contains residues 459 to 607 of the ORF2 protein (33), which is much longer than a linear antigenic epitope, suggesting that the neutralization epitope is conformational. Therefore, the detailed structure of the HEV capsid protein is required in order to understand the organization of HEV epitopes.

Currently, there are 1,600 HEV genomic sequences available through the International Nucleotide Sequence Database Collaboration. They are classified into four genotypes which vary by geographic distribution and host range (10). In contrast, only a single serotype has been identified, suggesting that the immunodominant domain of HEV is highly conserved among genotypes. Antibodies from any one of the four genotypes cross-react with the capsid protein of genotype 1 (7).

Like other hepatitis viruses, HEV does not propagate well in currently available cell culture systems. Hepatitis E preventive strategies so far rely on the use of ORF2-derived recombinant protein (16). When expressed in insect cells, recombinant truncated ORF2 protein (PORF2), with 52 residues deleted from

* Corresponding author. Mailing address: Molecular and Cellular Biology, University of California, 1 Shields Ave., Davis, CA 95616. Phone: (530) 752-5659. Fax: (530) 752-3085. E-mail: rhch@ucdavis.edu.
† These authors contributed equally.
▽ Published ahead of print on 10 November 2010.

the C terminus and 111 residues deleted from the N terminus, self-assembles into virus-like particles (VLPs) (15). Our previous structural analysis of recombinant HEV VLP by cryoelectron microscopy (cryo-EM) provided the first understanding of the quaternary arrangement of PORF2.

The essential assembly element of the PORF2 protein contained amino acids 125 to 600 (13), and the reconstructed VLP displayed a T=1 icosahedral particle composed of 60 copies of truncated PORF2 (30). Recently, crystal structures were reported for genotype 1 T=1 VLPs (31), genotype 3 T=1 VLPs (32), and genotype 4 T=1 VLPs (8), revealing that PORF2 is composed of three domains, the S domain, M domain, and P domain. The T=1 icosahedral shell is composed of 60 copies of S domains, while the M domain binds tightly to the S domain and interacts with two 3-fold-related M domains to form a surface plateau at each of the 3-fold axes. Two P domains are tightly associated as a dimeric spike that protrudes from each of the icosahedral 2-fold axes. As a result, on a low-resolution cryo-EM density map, the HEV T=1 VLP appears as an icosahedral particle with 30 spikes (30).

Although these VLPs are smaller (270 Å in diameter) than the native HEV virion (320 to 340 Å), oral administration of HEV VLPs to experimental animals can induce anti-HEV antibodies that bind to native HEV (14). When a B-cell tag of 11 amino acids on glycoprotein D of herpes simplex virus was covalently coupled to the C-terminal end of PORF2 (after residue 608), the fusion protein retained the ability of PORF2 to assemble and form chimeric T=1 icosahedral VLPs that were capable of eliciting systemic and mucosal antibodies against both HEV capsid protein and the attached B-cell tag (20). Therefore, the HEV T=1 VLP is a potential carrier for delivering not only HEV antigen but also foreign antigens or antiviral drugs to the host immune system. However, rational design of HEV-based delivery vectors requires detailed information on HEV VLP structure, as well as on HEV immunodominant domains.

Here, we identified antigenic structures using cryo-EM and three-dimensional reconstruction. Our results indicate that the binding footprint of a neutralizing antibody covers the lateral side of the P domain, while a B-cell tag at the C terminus does not alter the assembly of T=1 HEV VLP.

MATERIALS AND METHODS

Production and purification of anti-HEV monoclonal antibody (MAb) MAb224. Eight-week-old female BALB/c mice were immunized at 0 and 4 weeks by intraperitoneal inoculation with HEV VLPs (100 μg/ml). Four weeks later, a final boost containing an equal volume of antigen was administered. Three days after the final boost, mouse spleen cells were fused with P3U1 mouse myeloma cells using polyethylene glycol 1500 (50% [wt/vol]) (Boehringer, Mannheim, Germany) essentially as described by Adler and Faine (1). Supernatants from microplate wells positive for hybridoma growth were screened by enzyme-linked immunosorbent assay (ELISA) using recombinant HEV VLPs as the antigen. Hybridomas that secrete antibodies specific for HEV were subcloned three times by limiting dilution, after which they were considered to be monoclonal. Antibodies in the supernatants were isotyped using a mouse monoclonal antibody isotyping kit (Amersham, Little Chalfont, Buckinghamshire, United Kingdom) in accordance with the manufacturer's protocol. Hybridomas were grown in bulk in stationary flasks (Nunc, Roskilde, Denmark) using RPMI 1640 with 15% fetal calf serum. Antibodies were purified from cell supernatants using HiTrap protein G affinity columns (Pharmacia Biotech AB, Uppsala, Sweden) and stored at −80°C. Among all of the antibodies that were generated, MAb224, an immunoglobulin G1 (IgG1) isotype, was chosen for structural analysis.

Preparation of Fab224 fragments. Isolated Fab224 fragments were prepared from purified mouse monoclonal antibodies by papain cleavage. A reducing L-cysteine buffer was used to activate the papain, and MAb224 was mixed with papain at a molar ratio of 100:1. The mixture was incubated overnight at 30°C. The reaction was stopped by the addition of iodoacetamide, and the product was analyzed by SDS-PAGE. The Fab224 fragments were purified using a 5-ml prepacked protein A chromatography column (Pierce Protein Research) according to the manufacturer's instructions. The Fc fragments and uncleaved MAb224 antibodies were trapped in the column due to their affinity for protein A, while the Fab224 fragments were collected in the flowthrough fraction.

Production and purification of anti-HEV Fab4. Fab4 was prepared by phage display and purified according to the protocol described previously (25). Briefly, chimpanzee 1441 was infected with HEV strain SAR-55. Bone marrow was aspirated from the iliac crest of this animal, and the antibody κ-chain gene and γ1-chain gene were amplified and cloned into the pComb3H phage display vector and pGEM-T cloning vector (Promega), respectively, and transformed into *Escherichia coli* XL-1 Blue. The bacteria were then amplified and infected with helper phage VCS M13 at a multiplicity of infection of 50 to produce a library displayed on the surfaces of phage particles. Phage was panned on SAR-55 ORF2-coated ELISA wells; four rounds of panning were performed. After amplification of the selected library, the phagemid DNA was extracted and the vector was modified to remove the bacteriophage coat protein III-encoding region of the phage. The phagemid DNAs were religated and transformed into *E. coli* XL-1 Blue to produce soluble Fabs. The vector pComb3H was constructed to encode a six-histidine tail at the end of the Fab fragment, thus facilitating Fab purification. Fab4 purity was determined by SDS-PAGE, followed by colloidal Coomassie brilliant blue staining.

Production and purification of HEV VLPs. The production and purification of HEV VLPs were conducted as described previously (13, 15, 20, 30). Briefly, DNA fragments encoding the N-truncated ORF2 protein (for the wild-type VLP) and the chimeric ORF2 protein (for VLP-C-tag) were cloned using the baculovirus transfer vector pVL1393 to yield pVLORF2. Insect Sf9 cells (Riken Cell Bank, Tsukuba, Japan) were used to produce recombinant baculovirus. Tn5 insect cells were infected with the recombinant baculoviruses at a multiplicity of infection of 5 and incubated in Ex-Cell 405 medium (JRH Biosciences, Lenexa, KS) for 6 days at 26.5°C. The supernatant was collected after the removal of cell debris by centrifugation at 10,000 × *g* for 90 min. The HEV VLPs were pelleted at 100,000 × *g* for 2 h in a Beckman SW32 Ti rotor and resuspended in 4.5 ml Ex-Cell 405. The VLPs were further purified by centrifugation through a CsCl density gradient (1.31 g/ml) at 110,000 × *g* for 24 h at 4°C in a Beckman SW 55 Ti rotor. The white virus band was collected and diluted 4 times with Ex-Cell 405 to decrease the CsCl concentration, and then the VLPs were centrifuged for 2 h in a Beckman TLA 55 rotor at 100,000 × *g*. The VLPs were resuspended in 100 to 500 μl of 10 mM potassium-MES (morpholineethanesulfonic acid) buffer (pH = 6.2) and stored at 4°C. To construct chimeric VLP-C-tag, recombinant baculoviruses were prepared by inserting the B-cell tag epitope from herpes simplex virus glycoprotein D (QPELAPEDPED) at amino acid position 608 (20).

Western blotting. A series of DNA fragments were constructed to encode truncated ORF2 residues 112 to 660, 112 to 608, 112 to 602, 112 to 601, 112 to 600, 112 to 596, and 112 to 589. These recombinant ORF2 genes were inserted into a baculovirus vector and expressed in insect cells using the protocol for VLP production, except that the recombinant proteins were recovered from the cytoplasm after lysis of the cell. Recombinant proteins were heated in 4× Laemmli sample buffer and electrophoresed under reducing conditions in a 10% SDS–polyacrylamide gel. After transfer of proteins to a polyvinylidene difluoride (PVDF) membrane, the membrane was blocked with TBS buffer (20 mM Tris, pH 7.6, NaCl) containing 0.5% Tween 20 (vol/vol) prior to overnight incubation with Fab224 fragments at a 1:10 dilution. After extensive washing with TBS buffer containing 0.05% Tween 20 (vol/vol), alkaline phosphatase-conjugated anti-mouse IgG (Fab specific) was incubated with the membrane for 1 h at room temperature. The blot was then washed and developed with the *p*-nitroblue tetrazolium-5-bromo-4-chloro-3-indolylphosphate (NBT-BCIP) reaction.

Preparation of VLP-Fab complexes for cryoelectron microscopy. The VLP-Fab complexes were prepared by incubating Fabs with VLPs at a molar ratio exceeding 1:300 (VLP versus Fabs) at 4°C overnight. To reduce the background density in the subsequent structural determination, highly pure VLP-Fab complexes were obtained using a short column containing Sephacryl 300, which resulted in the removal of the unbound Fab from the sample. The fractions containing VLP-Fab complexes were collected based on their optical density readings at a wavelength of 280 nm. The Fab binding occupancy was roughly estimated by performing SDS-PAGE (8-to-25% gradient) on the purified VLP-Fab complexes at a constant voltage using the Phast system (Pharmacia). The

particle morphology of VLP-Fab complexes was examined by negative-stain electron microscopy using 2% uranyl acetate.

Cryoelectron microscopy. Sample preparation and cryo-EM were performed following previously described, well-established procedures (13, 30). Briefly, a drop containing 3.5 μl of the sample was applied to a glow-discharged holey carbon-coated copper grid, blotted with a piece of filter paper for 3 s to remove the extra liquid, and quickly plunged into liquid ethane cooled by liquid nitrogen. Samples were frozen in a thin layer of vitrified ice. The grid was then transferred into a Gatan 626DH cryo holder and kept at a low temperature (−178°C) during the subsequent data collection. Micrographs were collected under low-dose conditions (<10 e^{-}/Å^2) using Kodak SO163 film at a magnification of ×45,000 on an FEI CM-120 electron microscope operated at 120 kV, and particles were photographed at a defocus range of 1,000 to 3,000 nm. Micrographs were visually inspected and selected based on a suitable particle concentration, optimal ice thickness, and minimal specimen drift. Only micrographs fulfilling these criteria were analyzed.

Image processing. Selected micrographs were digitized using a Heidelberg Primescan D8200 (Heidelberg, Germany) at a 14-μm scanning step size, corresponding to 3.11 Å per pixel of specimen space. Particles were manually picked and centered by cross-correlating each one against the circular average image. The astigmatism and defocus value were evaluated by the superimposed power spectra from all particles within a single micrograph. The contrast transfer function's first zero was approximately within the range of 17 to 20 Å^{-1} for the data used for the structural determination. The self-common-lines algorithm (4) was used to yield the initial models for VLP-C-tag, VLP-Fab4, and VLP-Fab224. The origin and orientation search for each particle was carried out iteratively using the polar Fourier transformation (PFT) algorithm running on an AMD MP1800 MHz dual-processor Linux workstation (2). Three-dimensional reconstructions were computed by combining a set of particles with orientations that spread evenly in an icosahedral asymmetric unit using the Fourier-Bessel algorithm and by superimposing 5-3-2 icosahedral symmetry. To examine the reliability of the three-dimensional reconstruction, the data set was evenly divided into two parts at the final refinement step and two three-dimensional reconstructions were computed. The resolution was estimated using Fourier shell correlation (FSC) by assessing the agreement between these two reconstructions in Fourier space. Using a coefficient value of 0.5 as the criteria, the estimated resolutions of the three-dimensional reconstructions of VLP-C-tag, VLP-Fab224, and VLP-Fab4 were computed as 17.5 Å, 18.5 Å, and 24 Å, respectively.

The three-dimensional reconstructions were rendered and visualized using the Chimera program (22). The contour level was chosen at a value corresponding to 100% of the mass of the PORF2 protein. The electron density map was displayed in the isosurface mode, which builds a barrier to contour the density about a certain threshold.

Fitting the crystal structure into cryo-EM density maps. The density of the bound Fab molecule was determined from a difference density map, which was calculated by subtracting the cryo-EM map of unbound HEV T=1 VLP from the density map of the Fab-VLP complex. The cryo-EM map of unbound HEV VLP was published previously (30). Because the cryo-EM data for unbound VLP and the Fab-VLP complex were collected with the same FEI CM-120 electron microscope under similar imaging conditions, the difference density map was calculated by direct subtraction of the density of unbound VLP from the reconstruction of the Fab-VLP complex after normalizing the contrast between the two maps. The calculated difference map was used as a constraint in model fitting. Manual fitting was carried out by translational and rotational movement of the three-dimensional crystal structure of the PORF2 protein (PDB ID 2ZZQ) (31) into the cryo-EM density maps using program O (9). To obtain the best fit, the atomic model of the PORF2 subunit was treated as a rigid body. The fitting was first manually refined by minimizing the crashes between symmetry-related PORF2 molecules and then evaluated based on the cross correlation coefficient (CC value) between the cryo-EM density and the density computed from the fitted PORF2 coordinates. Fitting was halted when the CC value reached 80%. The figures were prepared using the program PyMOL (5), and the surface stereographic projection of the HEV VLP was prepared using the program RIVEM (29).

RESULTS

Binding of antibody MAb224 to PORF2. The binding of the monoclonal antibody Fab224 to PORF2 was examined via immunoblot analysis. A series of recombinant ORF2 proteins with C-terminal truncations were separated by SDS-PAGE on a 10% gel under reducing conditions and blotted with Fab224 (Fig. 1A). Fab224 recognized both reduced and denatured recombinant ORF2 proteins that contained amino acids 112 to 660, 112 to 608, 112 to 602, and 112 to 601. In contrast, recombinant ORF2 proteins composed of residues 112 to 600, 112 to 596, and 112 to 589 did not bind to Fab224. These data indicate that residues 597 to 601 are critical for Fab224 binding to PORF2. Because the recombinant ORF2 proteins were recovered from cell cytoplasm where multiple forms of PORF2 were reported (15), the positive bands observed at a low molecular weight may be the proteolytic products or degraded forms of ORF2 that contain the Fab224 binding sequence.

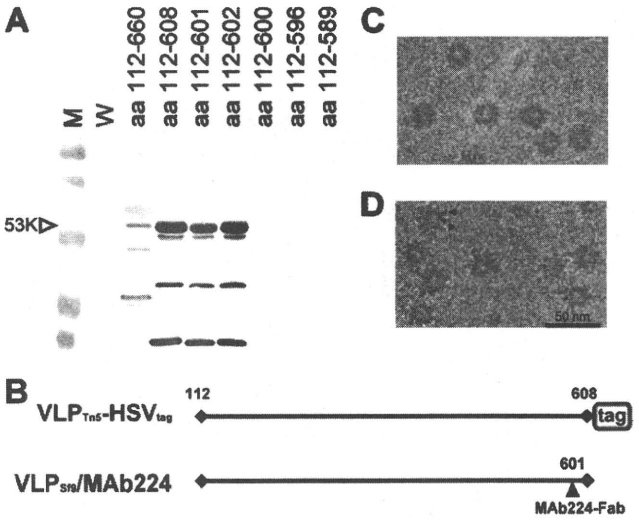

FIG. 1. Characterization of VLP-C-tag and VLP-Fab224. (A) Western blot assay of the C-terminally truncated ORF2 proteins with Fab224. M, molecular weight markers; W, peptides recovered from baculovirus-infected cells. (B) Diagram of the C-terminal markers. (C) Electron micrograph of frozen-hydrated VLP-C-tag. (D) Electron micrograph of frozen-hydrated VLP-Fab224. Black arrowheads indicate the Fab molecules attached to the VLP. Both particles showed an absence of density in the center. Note that the surface spikes in VLP-Fab224 appeared as longer thorn-like densities compared to those of VLP-C-tag.

Two-dimensional electron cryomicrographs. The chimeric VLPs (Fig. 1C) and the Fab224-conjugated VLP complex (Fig. 1D) showed circular profiles with spike-like densities that extended from the surface. As we observed previously (15, 30), they appeared to have a white, contrasting center, indicating that they are empty particles lacking RNA (data not shown). The sizes of both VLPs were approximately 27 nm without taking into account the extra densities that extended from the VLP-Fab224 surface (Fig. 1D).

Binding site of antibodies. The cryo-EM structure of HEV-Fab224 was reconstructed from 615 images of individual particles and displayed T=1 icosahedral symmetry with 60 protein subunits that were arranged into 30 dimeric protruding spikes located at each icosahedral 2-fold axis (Fig. 2A). Sixty Fab molecules were observed around each VLP particle, bound to the shoulder of the P domain. The Fab density extended ~57 Å radially away from the spike surface. The density corresponding to the Fab was approximately equal in magnitude to that of the HEV VLP, indicating that most or all of the 60

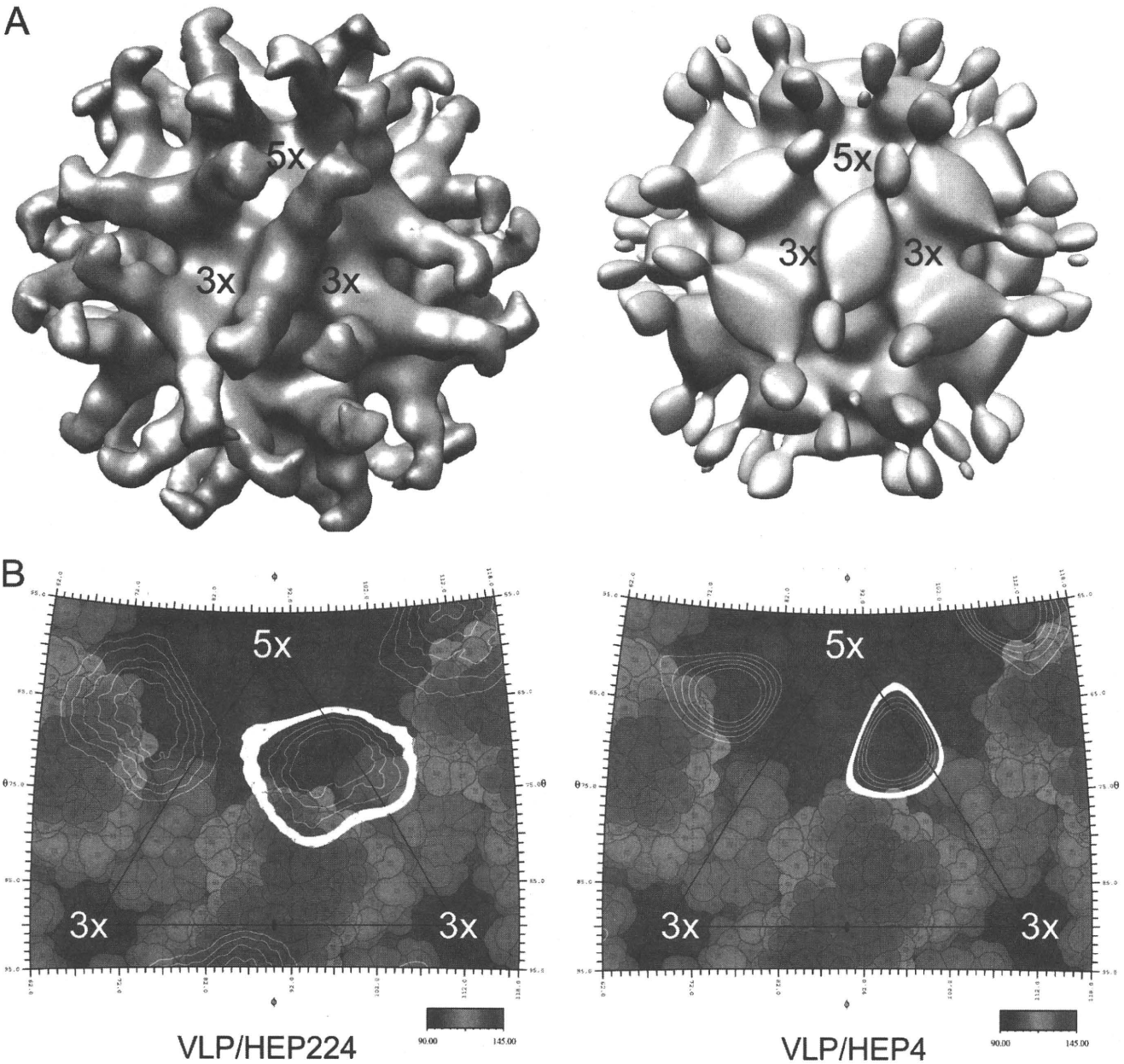

FIG. 2. The cryo-EM structure of HEV T=1 VLP in complex with anti-HEV antibodies. (A) Surface presentation of VLP-Fab224 (left) and VLP-Fab4 (right) viewed along one of the icosahedral 2-fold axes. One 5-fold axis and two adjacent 3-fold axes are marked with the corresponding number. In both reconstructions, 60 copies of Fab are attached to the lateral side of HEV VLP; however, the density of Fab4 molecules appears to be less than that of Fab224 molecules. (B) The viral surface is shown as a stereographic projection overlapped with a line drawing of an icosahedral asymmetric unit. The 5-fold and two adjacent 3-fold axes are marked with corresponding numbers, while the black triangle encloses the area of an icosahedral asymmetric unit. The surface residues are colored according to the distance from the center of the VLP, with red being the furthest away and blue representing the surface depressions. The Fab density is projected as white contour lines on the viral surface, and the outermost layer of density is drawn as thick white contour lines.

binding sites were occupied by a Fab molecule. The density corresponding to the VLP capsid was removed from the cryo-EM map, producing a Fab differential density map that was used to pinpoint the binding site of the Fab224 antibody (Fig. 3A and B).

In addition, the structure of HEV VLP in complex with the neutralizing antibody Fab4 was determined by combining 264 individual images. Fab4 precipitates both the native HEV virion and recombinant PORF2 peptides, but the reaction depends on the presence of amino acids 597 to 607 (26). Three-dimensional reconstruction of the VLP-Fab4 complex showed 60 Fab molecules bound to each HEV VLP. Unlike the VLP-Fab224 complex, the density corresponding to Fab4 was about one-third of that of the capsid (Fig. 2A), suggesting that only 30 to 40% of the binding sites were occupied by the Fab. Moreover, the binding of Fab4 appeared to be deeper on the

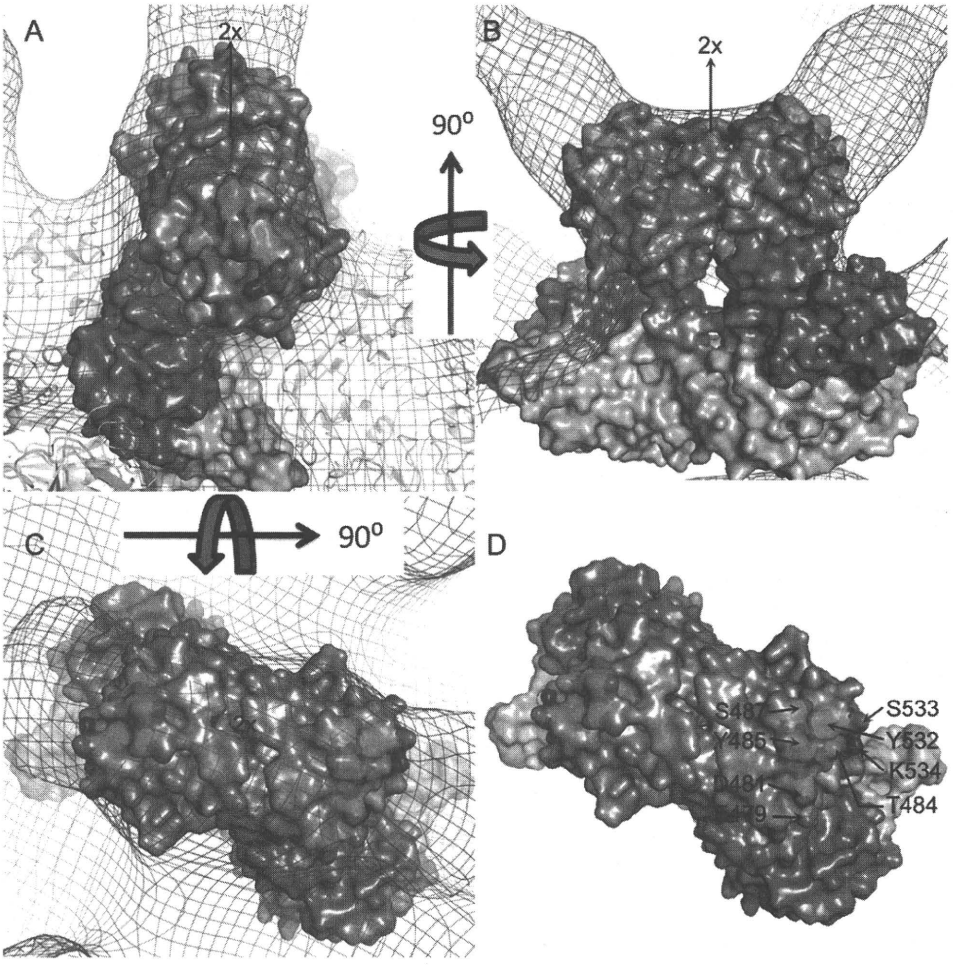

FIG. 3. The binding site of Fab224 antibody. (A) The cryo-EM density map of VLP-Fab224 was fitted with the crystal structure of PORF2 and viewed along a bound Fab molecule. One PORF2 dimer is presented as a solid surface and colored light magenta for the S domain, blue violet for the M domain, and dark gray for the P domain. The neighboring dimers are drawn in ribbon mode and colored wheat. (B) Side view of a PORF2 dimer fitted into the cryo-EM density map. (C) A PORF2 dimer viewed along the 2-fold axis and overlapped with the cryo-EM density map. (D) Top view of a PORF2 dimer viewed along the 2-fold axis. The amino acids in PORF2 responsible for binding to Fab224 are labeled. The PORF2 dimer is presented as a solid surface and colored in gray, violet, and light magenta for the P domain, the M domain, and the S domain, respectively. The residues along the Fab binding interface are colored according to the element, with green for carbon, blue for nitrogen, and red for oxygen.

side wall of the protruding domain toward the capsid shell, leaving its Fc domain exposed above the surface of the plateau (Fig. 2A). In contrast, the entire Fab224 molecule stood mainly on the top of the P domain surface. The Fab224 and the Fab4 molecules extend along the long axis of the P domain. In both cases, no steric hindrance of the Fab on the P domain with the neighboring Fab molecules at either the 5-fold or the 3-fold axes was apparent. The orientation of the Fabs relative to the plateau appeared different at a radius of 135 Å. The long axis of Fab224 tilted toward the neighboring spike, while the long axis of Fab4 pointed to the 5-fold axis (Fig. 2A).

To further analyze the Fab and HEV VLP binding interface, the crystal structure of genotype 1 PORF2 was docked onto the VLP-Fab224 cryo-EM density map. The genotype 1 PORF2 crystal structure (PDB ID 2ZZQ) is composed of three domains (31), and these domains are in good agreement with those of genotype 3 and genotype 4 PORF2 (PDB ID 2ZTN and 3HAG, respectively) (8, 32). The coordinates fitted very well with the cryo-EM density map without any adjustment (CC value of 80%). The atoms on the surface of the HEV VLP capsid were plotted and colored according to their radial distance and overlapped with the density of the Fab at the surface plateau of the protruding spike (Fig. 2B).

The Fab224 interacted with the residues on the side of the ORF2 spike rather than with those residues on the spike's plateau surface (Fig. 3C). The contact footprint did not overlap with the dimeric interface of the PORF2 spike. As expected, Fab224 recognizes a conformational epitope, and its binding site covers a surface composed of three loops, including amino acids 470 to 493 in AB loop, amino acids 539 to 569 in CD loop, and amino acids 581 to 595 in EF loop (Fig. 3D). Residues E479, D481, T484, Y485, and S487 from the AB loop and residues Y532, S533, and K534 from the CD loop were in close contact with the Fab molecule.

Structure of HEV chimeric VLP. Chimeric HEV VLP-C-tag was constructed using a PORF2 fusion protein in which a